Progress in Polymer Science 153 (2024) 101830

Contents lists available at ScienceDirect

Progress in Polymer Science

journal homepage: www.elsevier.com/locate/progpolymsci

Architecting MXenes in polymer composites

Huaixuan Cao[a], Natalie N. Neal[b], Savannah Pas[a], Miladin Radovic[b], Jodie L. Lutkenhaus[a,b], Micah J. Green[a,b,*], Emily B. Pentzer[b,c,*]

[a] Artie McFerrin Department of Chemical Engineering, Texas A&M University, College Station, TX USA
[b] Department of Materials Science and Engineering, Texas A&M University, College Station, TX USA
[c] Department of Chemistry, Texas A&M University, College Station, TX USA

ARTICLE INFO

Article history:
Received 6 February 2024
Revised 27 April 2024
Accepted 2 May 2024
Available online 3 May 2024

Keywords:
Composite
MXenes
Processing-structure-application relationships
Films
Foams

ABSTRACT

MXene/polymer composites are attractive materials and find extensive use in many applications, such as energy storage, electromagnetic interference (EMI) shielding, membranes, catalysis, sensors, and biomedicine. The major challenge to fabricate MXene/polymer composites are the processing conditions and poor control over the distribution of the MXene nanosheets within the polymer matrix. Traditional ways involve the direct mix of fillers and polymers to form a random homogeneous composite, which leads to inefficient use of fillers. To address these challenges, researchers have focused on the development of ordered MXene/polymer composite structures using various fabrication strategies. In this review, we summarize recent advances of structured MXene/polymer composites and their processing-structure-property relationships. Two main forms of MXene/polymer composites (films and foams) are separately discussed with a focus on the detailed fabrication means and corresponding structures. These architected composites complement those in which MXenes nanosheets are isotropically dispersed throughout, such as those formed by aqueous solution mixing approaches. This review culminates in a perspective on the future opportunities for architected MXene/polymer composites.

1. Introduction

Polymer nanocomposites are composed of polymer matrix and nanoparticle filers and are highly attractive due to the combined properties of both components. Specifically, polymers are easy to process, flexible, lightweight, and low-cost, whereas nanoparticles can possess excellent electrical [1,2], thermal [3,4], catalytic [5], and magnetic properties [6], critical to a variety of advanced applications. The nanoparticle fillers may be different shapes and aspect ratios, but are most commonly spherical, rod-like, or sheet-like with at least one dimension that is <100 nm. Sheet-like 2D nanoparticle fillers are distinct due to their unique planar nature (which allows for assembly on 2D surfaces) and large lateral dimensions, as well as high aspect ratio, anisotropic properties, and high surface area [7–9]. 2D nanoparticles are usually single to few atomic layers thick with the lateral size up to micrometers. Examples of 2D nanoparticles that have been used as fillers in polymer nanocomposites include graphene, graphene oxide (GO), transition metal dichalcogenides, and transition metal oxides; more recently, MXenes, or transition metal carbide, nitrides, or carbonitrides have emerged as revolutionary 2D nanofillers for polymer composites [7,10].

Mxenes have intriguing electronic, mechanical, and catalytic properties and versatile chemistries [11–13], and can be processed in solution or in melt for polymer composites. The general formula to MXenes is $M_{n+1}X_nT_z$, where M is transition metal (e.g., Ti, V, Nb) and X is carbon or nitrogen, and T_z are terminal groups (e.g., -OH, -F, -Cl, -Br). The available combinations of M and X give versatile composition of MXenes, with $Ti_3C_2T_z$ being the most commonly studied MXene. These nanosheets are usually synthesized by selective etching of the bonded A layer from their parent MAX phase, where A is group 13 or 14 elements from the periodic table, such as Al [14]. Wet chemical

Abbreviations: ANF, Aramid nanofibers; CNT, carbon nanotube; CNF, cellulose nanofiber; EMI, electromagnetic interference; GO, graphene oxide; HA, hyaluronic acid; HAP, hydroxyapatite; HIPEs, high internal phase emulsions; IL, ionic liquid; LbL, layer-by-layer; LP, layer pair; NR, natural rubber; PAmA, poly(amic acid); PANI, polyaniline; PDAC, diallyldimethylammonium chloride); PDDA, polydiallyldimethylammonium chloride; PDMS, poly(dimethyl siloxane); PEDOT-PSS, poly(3,4-ethylenedioxythiophene)-polystyrene sulfonate; PEG, polyethylene glycol; PET, poly(ethylene terephthalate); PI, polyimide; PMMA, poly(methyl methacrylate); PP, polypropylene; PS, polystyrene; PU, polyurethane; PVA, polyvinyl alcohol; PVC, polyvinyl chloride; PVDF, polyvinylidene fluoride; rGO, reduced graphene oxide; RF, radio frequency; AgNW, silver nanowire; SA, sodium alginate; TAEA, tris(2-aminoethyl)amine; TPU, thermoplastic polyurethane; VAF, vacuum-assisted filtration.

* Corresponding authors.
E-mail addresses: micah.green@tamu.edu (M.J. Green), emilypentzer@tamu.edu (E.B. Pentzer).

https://doi.org/10.1016/j.progpolymsci.2024.101830
0079-6700/

etching using HF is commonly used for the synthesis of MXenes and gives nanosheets with surfaces terminated with -O-, -F, and -OH and a high negative ζ-potential. This composition makes MXenes readily dispersible in water and the terminal groups offer possibilities for surface functionalization, increasing the versatility of MXenes. In addition to the fluorine-containing acid etching approach, molten salt etching has been developed recently (e.g., using $ZnCl_2$ and $CuCl_2$) [15–17], which expands the synthetic pathways. MXenes offer metallic conductivity (up to *2000,000 S/m*) and effective electromagnetic absorption [11,18], rendering them as extraordinary fillers in polymer composites. In recent years, MXene/polymer composites have gained increasing attention for applications across energy storage, catalysis, electromagnetic interference (EMI) shielding, sensing, biomedicine, and membranes [19–22]. To date, MXenes have most commonly been incorporated into commercially available common polymers including polyvinyl alcohol (PVA) [23–25], polyacrylamide [26,27], polydiallyldimethylammonium chloride (PDDA) [28], polyvinyl chloride (PVC) [29], poly(3,4-ethylenedioxythiophene)-polystyrene sulfonate (PEDOT-PSS) [30,31], polyvinylidene fluoride (PVDF) [32–34], thermoplastic polyurethane (TPU) [35,36], polystyrene (PS) [37,38], natural rubber (NR) [39,40], polypropylene (PP) [41,42], and cellulose [43].

The major challenges in preparing MXene/polymer composites are suitable processing conditions and control over the structure within the resulting composite (i.e., orientation and ordering of the nanosheets). The most common fabrication methods for MXene/polymer composites involve the direct mixing of polymer and MXenes in solution, e.g., solution casting, or in the melt, e.g., melt blending. For example, MXene/polymer films can be fabricated by mixing solutions of MXene and polymer then doctor blading or spin coating, and solvent evaporation. In the case of melt blending, polymer and MXenes are combined above a temperature at which the polymer freely flows. In solution mixing, a common solvent is required (e.g., water), and in melt processing (e.g., at elevated temperature), care must be taken to prevent oxidation of MXene nanosheets into the analogous metal oxide [44]. In these traditional methods of processing MXene/polymer composites, nanosheets may aggregate and phase separate from the polymer due to the strong inter-nanosheet van der Waals interactions;[45] further, both approaches typically lead to randomly distributed MXenes within the polymer matrix, which limits structure tunability and comprehensive evaluation of structure-property relationships. Numerous prior reviews have addressed such homogeneous systems [44,46–49]. To address the limitations of MXene-polymer composite composition and structure, various fabrication strategies have been reported to architect MXene nanosheets within a polymer matrix [45,50,51], thereby controlling the microscopic and/or macroscopic structure of MXene/polymer composites and potentially enhancing performance-related properties, en route to producing more effective and sustainable devices critical to addressing a variety of societal needs.

This review summarizes the current state-of-the-art understanding of processing-structure-property relationships of MXene/polymer composites in which MXene nanosheets are architected throughout the polymer matrix (meaning having an organized distribution and/or orientation). Reviews of structured polymer composites with other fillers are available, such as structured graphene-based nanoparticle (graphene, graphene oxide, reduced graphene oxide (rGO))/polymer composites [52–54], and carbon nanotube(CNT)/polymer composites [55,56]. In this review, the processing methods and their corresponding structures for MXene/polymer composites are discussed in detail. Specifically, we address structured MXene/polymer films and foams and their corresponding microscopic and macroscopic structures which include segregated compact films, layered films, networked films, directional foams, coated foams, and emulsion-templated foams (Fig. 1). Section 2 discusses MXene/polymer films and is organized by four common fabrication methods: vacuum-assisted filtration (VAF), layer-by-layer assembly (LbL), particle processing, and polymer impregnation. Section 3 addresses MXene/polymer foams and is also organized by fabrication method: freeze drying, foaming agent, template coating, and polymerizations in emulsions. The review culminates with a perspective of the immediate needs and opportunities of architected MXene/polymer composites, provided in Section 4.

2. Architected MXene/polymer films

MXene/polymer composite films have been used in supercapacitors, for EMI shielding, membranes, and sensors, due to high volumetric capacitance, high electrical conductivity, high thermal conductivity, and efficient electromagnetic shielding properties [57–59]. In this section, we detail advances in the production of structured MXene/polymer films using four main fabrication methods, with a focus on how processing dictates the structure and how structure impacts desirable properties.

Fig. 2 outlines the four main fabrication strategies for MXene/polymer composite films and their corresponding characteristic composites structures. Vacuum-assisted filtration (VAF) utilizes pressure-driven flow to align the MXene nanosheets parallel to film surface within a polymer, resulting in a brick-and-mortar structure in which nanosheets are the brick and polymer is the mortar. In complement, layer-by-layer (LbL) assembly is used to fabricate alternating layers of MXene nanosheets and polymers by stepwise addition of each layer. Latex processing makes use of MXene-coated polymer particles and compression molding to fabricate segregated structures containing an interconnected MXene nanosheet network throughout. Lastly, polymer impregnation leverages pre-structured MXene monoliths to be infiltrated with polymer to create MXene/polymer architectures, again with a network of MXenes throughout the polymer.

2.1. Vacuum-Assisted filtration

VAF is a simple fabrication technique that is widely used to produce polymer nanocomposite with various fillers, including MXenes. Typically, a brick-and-mortar structure is formed through this process, again in which the MXene nanosheets are the bricks, providing good electrical properties, and the polymer is the mortar, binding the nanosheets together and giving good mechanical properties, which could potentially be beneficial for ultrathin film electronic applications, such as EMI shielding. This process requires a common good solvent for MXene and polymers; due to the high hydrophilicity and aqueous dispersibility of MXenes, hydrophilic polymers and aqueous solutions are commonly used. Hydrophobic polymers are less common and would require the use of polar organic solvents and/or modification of MXenes.

As an example of MXene-polymer composites from VAF, Liu et al. reported the formation of $Ti_3C_2T_z$/ PEDOT:PSS composite film with a brick-and-mortar structure [60]. As is shown in Fig. 3**a**, aqueous dispersions of $Ti_3C_2T_z$ nanosheets and PEDOT:PSS were mixed by ultrasonic stirring, then subjected to VAF to yield a free-standing $Ti_3C_2T_z$/PEDOT:PSS film. The SEM image of the cross-section of the composite film showed the multilayered structure with $Ti_3C_2T_z$ nanosheets as the inorganic brick framework and polymer as the organic mortar. These films had high electrical conductivity (34,000 S/m, with 87.5 wt% of $Ti_3C_2T_z$). More notably, the high amount of interface between the embedded PEDOT:PSS and nanosheets significantly enhanced the internal reflection and polarization for electromagnetic wave absorption (total

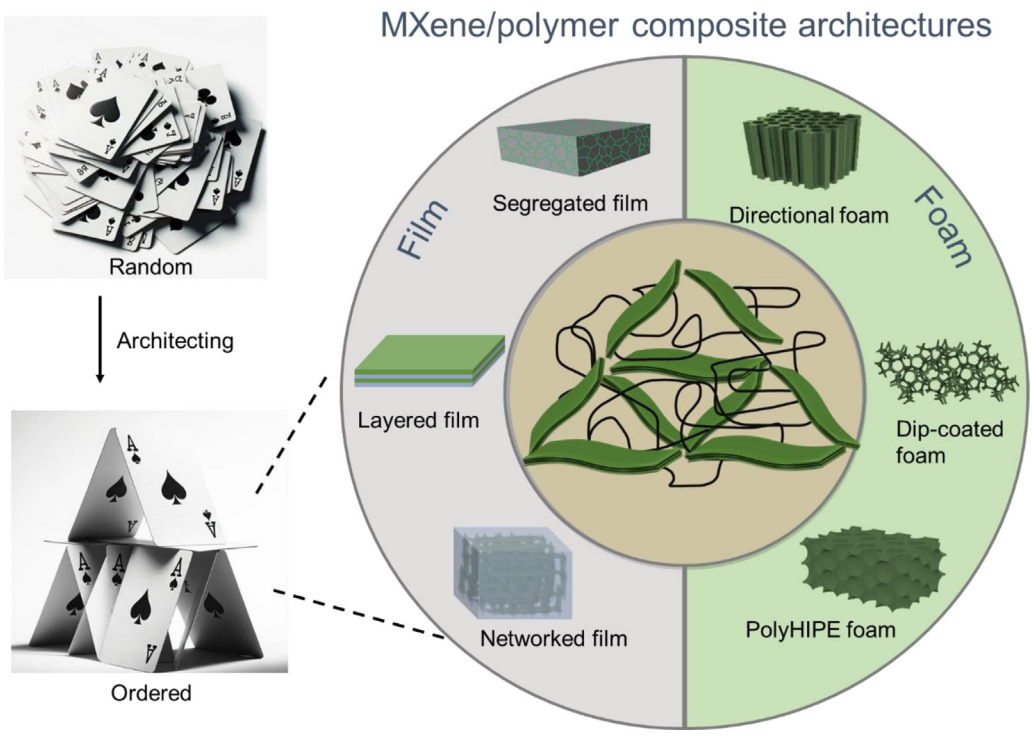

Fig. 1. MXene/polymer composite architectures that are compact films or porous foams. In contrast to a randomly oriented and aggregated collections of nanosheets, architected MXene/polymer structures contain nanosheet networks, nanosheet-lined pores, or anisotropic organization of nanosheets that can advance performance-related properties.

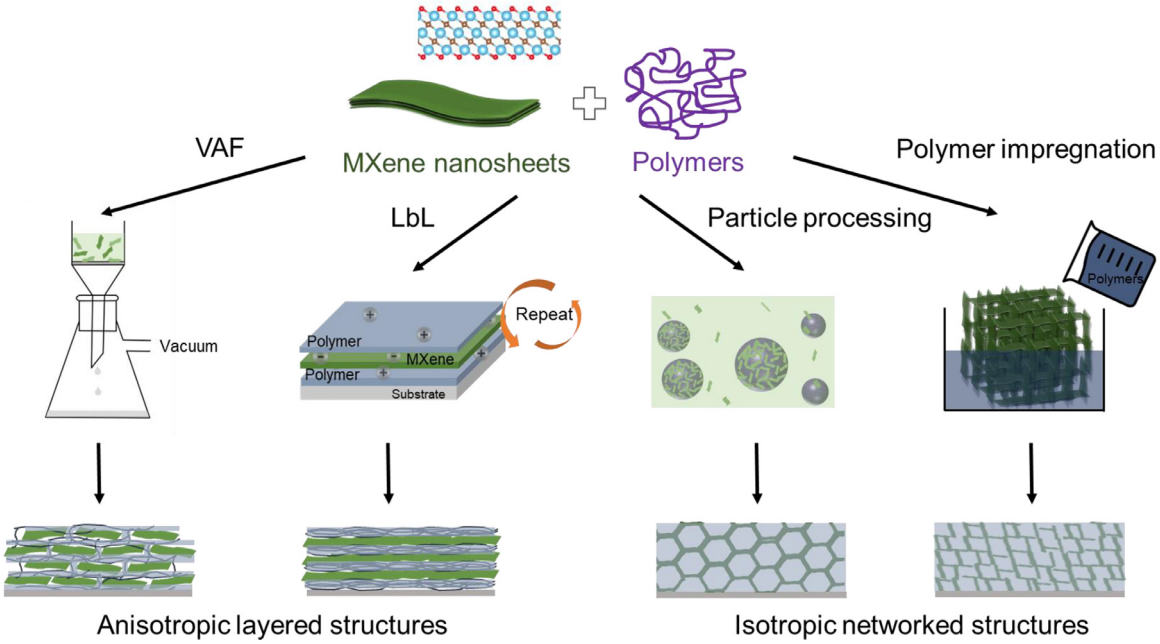

Fig. 2. Summary of the fabrication methods for structured MXene/polymer films. VAF method typically leads to brick-and-mortar structure of MXene and polymers. LbL assembly results alternating layers of MXene and polymers. Particle processing usually creates an organized framework of MXenes within polymer matrix. Polymer impregnation typically leads to a networked MXene structure filled with polymer matrix.

shielding effectiveness of 42.1 dB, absorption shielding effectiveness of ~28 dB for a 11.1 μm thick film). Similarly, $Ti_3C_2T_z$/PEDOT composite films can be prepared by VAF, followed by etching off the non-conductive PSS using H_2SO_4 [61], and the resulting $Ti_3C_2T_z$/PEDOT film exhibited high EMI shielding properties (40.5 dB for a 6.6 μm thick film with 70 wt% $Ti_3C_2T_z$). The VAF method has also been used fabricate $Ti_3C_2T_z$ MXene composite films with water-dispersible cellulose nanofiber (CNF) [62], and sodium alginate (SA) [63], for EMI shielding applications (24 dB, 47 μm film, 70 wt% of $Ti_3C_2T_z$ for $Ti_3C_2T_z$/CNF and 57 dB, 8 μm film, 90 wt% of $Ti_3C_2T_z$ for $Ti_3C_2T_z$/SA).

In the VAF process, non-covalent interactions between MXenes and the polymer matrix can play an important role in the composite structures. For example, Ling et al. fabricated $Ti_3C_2T_z$/polymer composite films with two different polymers: PDDA and PVA [64]. As illustrated in Fig. 3**b**, cationic PDDA electrostatically interacted

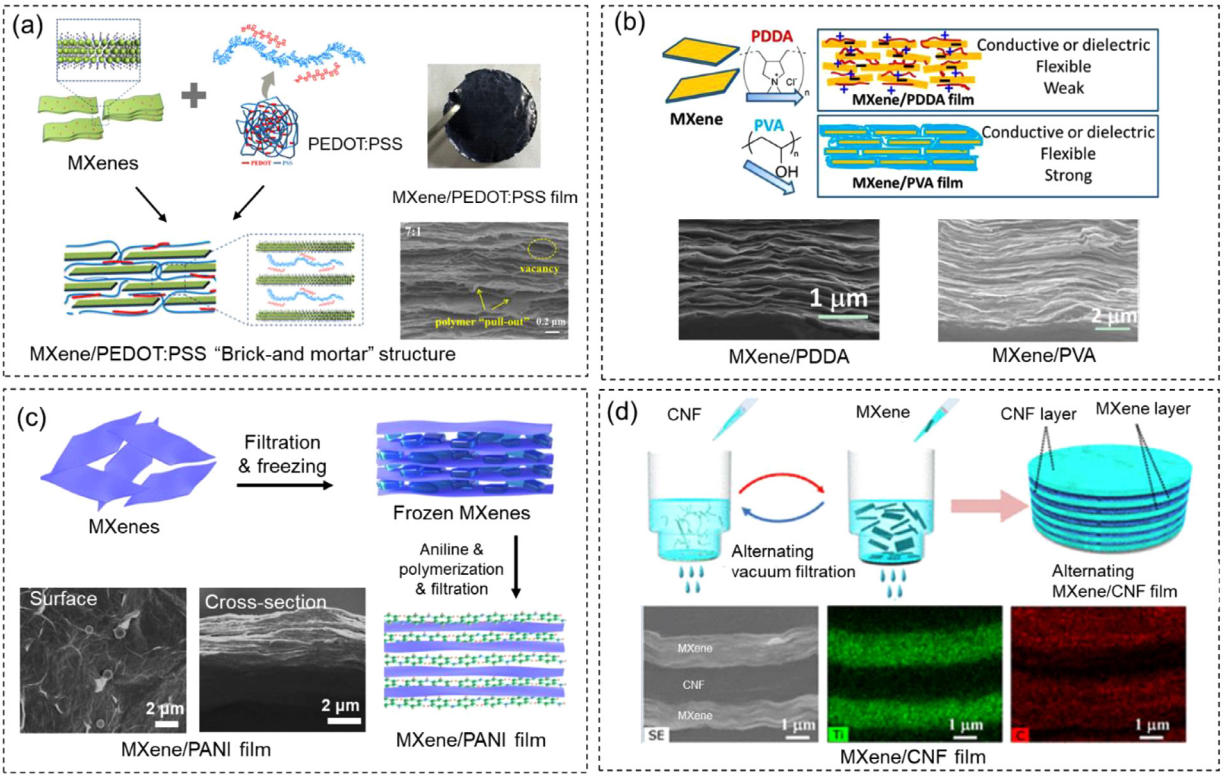

Fig. 3. MXene/polymer composite films prepared by VAF fabrication and their corresponding structures. (a) $Ti_3C_2T_z$/PEDOT:PSS film through VAF of $Ti_3C_2T_z$ and PEDOT:PSS. SEM image showing the cross-section of the composite film.[60] *Copyright 2018. Adapted with permission from American Chemical Society.* (b) VAF of $Ti_3C_2T_z$ with charged polymer (PDDA) or neutral polymer (PVA) and their different cross-sectional SEM images [64]. *Copyright 2014. Adapted with permission from National Academy of Sciences.* (c) $Ti_3C_2T_z$/PANI film via ice assisted VAF process and their surface and cross-sectional SEM images. This Figure is adapted from Ref [70]. *Copyright 2023. Adapted with permission from the Royal Society of Chemistry.* (d) The process of alternating VAF of $Ti_3C_2T_z$ and CNF for the fabrication of $Ti_3C_2T_z$/CNF layered structure and their SEM and EDS mapping images (Ti in green and C in red) [71]. *Copyright 2020. Adapted with permission from American Chemical Society.*

with negatively charged $Ti_3C_2T_z$ nanosheets, leading to adsorption of PDDA on the nanosheet surfaces; the resulting films had a relatively loose structure with some voids, and a similar layered structure as MXene-only film (left and middle SEM in Fig. 3**b**). Alternatively, in the $Ti_3C_2T_z$/PVA film, only hydrogen bonding interactions between the PVA and MXenes were possible, and the film had a compact layered structure. If negatively charged polymer is used, electrostatic repulsion between MXene nanosheets and the polymer results in better dispersion of the nanosheets. For example, Zhang et al. prepared composite films of negatively charged aramid nanofibers (ANFs) and $Ti_3C_2T_z$ nanosheets, observing a lamellar-like structure which the authors attributed to uniform dispersion of the two components due to electrostatic repulsion. Relevant to application in an osmotic membrane system, these composites show enhanced ion selectivity and ion flux compared to pristine $Ti_3C_2T_z$, which resulted in high power density (4.1 W/m^2) and conversion efficiency for osmotic energy harvesting; this was attributed to the synergetic effect of the surface charge of $Ti_3C_2T_z$ and the space charge of the ANFs [65]. Other composites prepared by VAF include $Ti_3C_2T_z$/silver nanowire (AgNW)/ANF films of one layer of $Ti_3C_2T_z$/AgNW and another layer of ANFs; this asymmetric two-layer structure exhibited high EMI shielding efficiency (35.5 dB) compared to homogeneous counterparts (9.8 dB for a homogeneous blended $Ti_3C_2T_z$/AgNW/ANF film with 10 wt% of $Ti_3C_2T_z$/AgNW) [66].

In situ polymerization of MXene/monomer solution can also be used in the VAF process. Typically, monomers and MXenes are mixed in solution and polymerization is induced before filtration. For example, Boota et al. reported the in situ polymerization of pyrrole in the presence of $Ti_3C_2T_z$ and subsequent VAF to make $Ti_3C_2T_z$/polypyrrole composite film [67]. Hydrogen bonding interactions between the N–H group of the pyrrole rings and O–H group of the $Ti_3C_2T_z$ surface led to the polymer chains aligning on the nanosheet surface. Similarly, aniline was polymerized in the presence of MXenes then VAF was used to prepare composite films [68], with or without oxidant [69]. Alternatively, Wang et al. used ice-assisted intercalation of aniline between $Ti_3C_2T_z$ nanosheets and subsequent polymerization and VAF for aligned $Ti_3C_2T_z$/polyaniline (PANI) films [70]. As shown in Fig. 3**c**, an aqueous dispersion of $Ti_3C_2T_z$ nanosheets was filtered then frozen. The frozen film was immersed in a solution of aniline monomer, followed by in situ oxidative polymerization of aniline. The polymerized mixture was isolated by VAF and a flexible $Ti_3C_2T_z$/polyaniline film with highly aligned structure was obtained (SEM in Fig. 3**c**). The freezing of the $Ti_3C_2T_z$ film helped to keep the structure intact during immersion and polymerization of aniline. Benefiting from the increased interlayer spacing from the polyaniline and $Ti_3C_2T_z$ layers, the $Ti_3C_2T_z$/polyaniline film exhibited high specific capacitance (gravimetric capacitance of 385 F/g) promising for flexible supercapacitor applications.

Alternating VAF is another important process for producing MXene/polymer composites with layered structures. For example, Zhou et al. reported $Ti_3C_2T_z$/CNF composites with alternating layers of MXene and CNF [71]. Fig. 3**d** shows the alternating vacuum filtration of one layer of CNF, followed by a second layer of $Ti_3C_2T_z$, and a third layer of CNF. The cross-sectional SEM image and EDS mapping demonstrated the distinct $Ti_3C_2T_z$ and CNF phases. This process enables the fabrication of highly oriented structure with good control of each layer thickness which impacts mechanical and electrical properties. For example, electrical conductivity de-

creased with an increase of $Ti_3C_2T_z$ layer numbers (from 621 to 82 S/m for 1 to 5 layers, though each had ~50 wt% $Ti_3C_2T_z$). Further, the conductivity was only 2 S/m for a homogenous mixture of $Ti_3C_2T_z$ and CNF with the same $Ti_3C_2T_z$ loading. The increased electrical conductivity afforded by the alternating structure holds promise for EMI shielding applications (40 dB for 4 layers of $Ti_3C_2T_z$ and 5 layers of CNF film). Utilizing a similar alternating VAF strategy, MXene/polymer films of $Ti_3C_2T_z$/AgNW/CNF[72] and $Ti_3C_2T_z$/AgNW/poly(dimethyl siloxane) (PDMS)[73] have been produced for EMI shielding applications (55.9 dB, 35 μm film, 50 wt% of fillers for $Ti_3C_2T_z$/AgNW/CNF and 50.82 dB, 1 μm film, 3.2 g/m^2 of fillers for $Ti_3C_2T_z$/AgNW/PDMS).

2.2. Layer-by-layer assembly

Layer-by-layer (LbL) assembly provides a simple way to architect layered MXene/polymer composites. Using non-covalent interactions, such as electrostatic interactions, charge-transfer interactions, and hydrogen bonding, LbL assembly creates multilayered films and coatings on a variety of substrates[74,75] by the alternating deposition of layers of complementary materials through immersion, spray-coating, or spin-coating. Between each deposition step, a washing/drying cycle is typically applied to remove loosely adhered material and prevent contamination of dispersions [76]. There is a vast history of charge solubilized polymers being used in LbL assembly with a layered structure, and due to the hydrophilic nature and negative ζ-potential of MXenes, they also make excellent LbL components [74,75,77,78]. Structures produced by LbL assembly with nanomaterials have layered structure, where each layer thickness has a resolution in the nanometer range, distinctly different from the brick-and-mortar structures produced by VAF which are a magnitude or two larger in thickness [60,61]. The customization of the LbL process allows for relatively easy manipulation of the nanostructure, such as through variation of the type of MXene, polymer type, deposition time, and the deposition technique (immersion-assisted, spray-assisted, or spin-assisted).

As a typical example of LbL assembly of MXene/polymer composite films or coatings, An et al. fabricated $Ti_3C_2T_z$/poly(diallyldimethylammonium chloride) (PDAC) multilayered composites [79]. As shown in Fig. 4**a**, a glass substrate was immersed in an aqueous PDAC solution, rinsed with DI water to remove the excess solution, then immersed in a $Ti_3C_2T_z$ solution, and finally rinsed with DI water. This process was repeated to obtain the composite film with desired thickness, based on the number of alternating $Ti_3C_2T_z$ and PDAC layers. Electrostatic attraction of positively charged PDAC and negatively charged $Ti_3C_2T_z$ assured the adhesion between layers and that no phase separation occurred. Digital images show the dark uniform coating of $Ti_3C_2T_z$/PDAC layers on the glass slide and SEM images indicate the well-aligned alternating multilayer pairs of $Ti_3C_2T_z$ and PDAC. The $Ti_3C_2T_z$/PDAC coating had good mechanical integrity. Notably, flexible substrates such as poly(ethylene terephthalate) (PET), PDMS, and nylon fibers can be used as substrates and hold promise for sensing applications (such as bending (up to 2.5-mm bending radius) and stretching (up to 40 % tensile strain)).

The nanostructure of the multilayered LbL films is highly dependent on the type of MXene. For example, Echols et al. investigated how the identity of MXene impacts film thickness growth [80]. In this study, LbL assemblies of Ti_2CT_z/PDAC and Nb_2CT_z/PDAC were prepared and compared to the previously reported $Ti_3C_2T_z$/PDAC. The average layer pair (LP) thickness was determined using profilometry, giving 3.9 ± 1.2 nm/LP, 7.3 ± 1.4 nm/LP, and 6.4 ± 1.3 nm/LP for the $Ti_3C_2T_z$/PDAC, Ti_2CT_z/PDAC, Nb_2CT_z/PDAC, respectively. The authors suggested that film growth is correlated with the ζ-potential of the MXenes. For example, MXenes with more negative ζ-potentials (−46.0 and −48.7 mV for Ti_2CT_z and Nb_2CT_z) exhibit higher growth rate compared to $Ti_3C_2T_z$ (−29.8 mV). This more negative ζ-potential may cause MXene nanosheets to be more strongly adhered to the previous layer of the film, preventing materials from being washed away and thus giving a thicker layer.

In addition to polycations, smaller molecules can also be utilized as the cationic layer for LbL assembly. Tian et al. reported the use of the small molecule tris(2-aminoethyl)amine (TAEA) for LbL assembly of $Ti_3C_2T_z$/TAEA composites;[81] the authors found that the use of TAEA created composites with more ordered and smoother multilayer structures (Fig. 4**b**) and minimized interlayer distance compared to LbL films made with larger polycations, like PDAC [79]. The small gap between MXene layers resulted in high electrical conductivity (7.3 × 10^4 S/m for 20 bilayers) and when the $Ti_3C_2T_z$/TAEA coating was deposited onto on PET substrate it exhibited high supercapacitor properties with 165 F/g at 2 mV/s using PVA/H_2SO_4 solid-state electrolyte.

In addition to composition, the processing parameters can also impact the architecture of the LbL MXene/polymer films, with deposition time significantly affecting distance between MXene layers. An et al. created $Ti_3C_2T_z$/PDAC LbL films with PDAC deposition times of 5, 10, and 15 min with same $Ti_3C_2T_z$ deposition time (15 min) [82]. The PDAC composition increases with increasing 5-minute intervals, 6.1 wt% (5 min), 7.8 wt% (10 min), 9.3 wt% (15 min). The greater loading of PDAC is reflected in the greater polymer layer thicknesses, causing the distance between the MXene layers to increase. This study also showed that the PDAC deposition was also sensitive to humidity, with thicker PDAC layers at higher humidity attributed to water intercalation in the polymer.

One downside to LbL deposition is the amount of time required to create multilayers. Alternatively, spray-coating and spin-coating can be used for LbL assembly of MXene/polymer composites. Weng et al. used a spin-spray LbL deposition method to rapidly create ($Ti_3C_2T_z$-PVA)/(CNT)-PSS) composites for EMI shielding [83]. As is shown in Fig. 4**c**, the multilayer composites were prepared by alternatively spraying two solution ($Ti_3C_2T_z$-PVA solution and CNT-PSS solution) onto a spinning substrate. The spin-spray LbL (ssLbL) method is not limited by diffusion processes as in the immersion method but gives layers less than a nanometer thick versus several nanometers thick. The SEM images in Fig. 4**c** show that the ssLbL layers are so thin that the cross-sectional SEM is unable to distinguish between the CNT-PSS and $Ti_3C_2T_z$-PVA due to resolution limits. Thus, ssLbL produces composites with much smaller distances between MXene layers, e.g., about one nanosheet thick versus several sheets in the layers of the immersion method [79,81,84]. The ssLbL-produced ($Ti_3C_2T_z$-PVA)/(CNT-PSS) composites exhibited high electrical conductivity (130 S/m for 300 bilayers) and efficient EMI shielding properties (3 dB for ~200 nm thick samples (300 bilayers)). In complement, Tian et al. used two different LbL assembly methods: spin-assisted immersion and vacuum-assisted spray LbL [81]. The selection of method was based on the substrate used: planar substrates (e.g., PET, glass slides, and Si wafers) lent themselves to the spin-assisted immersion LbL, whereas vacuum-assisted spray LbL was needed to penetrate porous 3D substrates (e.g., nonwoven fibers, cellulose paper, carbon nanofiber aerogel, and melamine foam) to create uniform coatings. The detailed discussion of LbL deposition of MXenes or polymers onto 3D skeleton is included in the foam section.

While the vast majority of LbL-assembled MXene/polymer composites rely on electrostatic interactions to create the multilayered structures, other non-covalent interactions can be used. For example, although hydrogen-bonding-driven LbL assembly has been thoroughly investigated for polymer-polymer composites [85–87], it has yet to be reported for MXene/polymer composites. However, hydrogen bonding interactions between MXenes and hydrophilic polymers (e.g., PVA) have been reported [88,89], and thus MX-

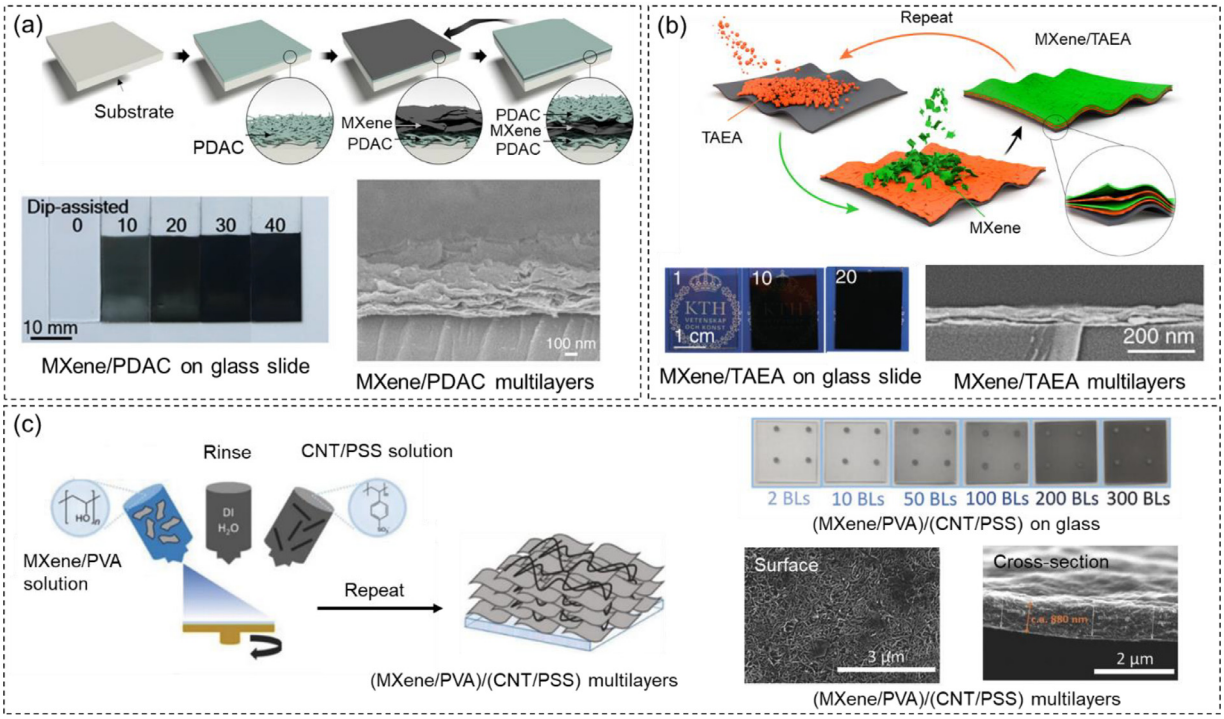

Fig. 4. MXene/polymer composite films prepared by the layer-by-layer (LbL) assembly method and their corresponding structures. (a) $Ti_3C_2T_z$/PDAC multilayer structures fabricated by immersion LbL assembly of PDAC and $Ti_3C_2T_z$, digital images of the $Ti_3C_2T_z$/PDAC multilayers on a glass substrate with different LP numbers, and SEM image of the cross-section of the $Ti_3C_2T_z$/PDAC multilayers [79]. *Copyright 2018. Adapted with permission from American Association for the Advancement of Science.* (b) Fabrication of $Ti_3C_2T_z$/TAEA using immersion LbL assembly and their corresponding digital images and SEM images [81]. *Copyright 2019. Adapted with permission from Springer Nature Limited.* (c) ($Ti_3C_2T_z$-PVA)/(CNT-PSS) composite film prepared by spray spin LbL assembly of a $Ti_3C_2T_z$-PVA solution and CNT-PSS solution. Digital and SEM images show uniform deposition of ($Ti_3C_2T_z$-PVA)/(CNT-PSS) multilayers and no obvious layer boundaries observed [83]. *Copyright 2018. Adapted with permission from John Wiley & Sons Inc.*

ene/polymer hydrogen bonded LbL multilayers should be feasible. Depending on the intended application, this may allow for more different polymers that can be used to be included into LbL MXene/polymer composites [87,90].

2.3. Particle processing

Segregated MXene/polymer composites can be created by particle processing methods. This method utilizes particles (e.g., polymer spheres) as templates, and the MXene nanosheets are confined at the particle surface. These composite particles can then be used for film formation, for example, using compression molding or filtration, giving organized MXene nanosheets within the polymer films with the initial particle serving as a template. In this approach, high electrical and/or thermal conductivity can be realized even at low MXene loading due to the interconnected MXene network within the polymer matrix [51,91,92]. To form the desired MXene network, nanosheets must be uniformly coated onto the polymer particles and must remain stable upon fusion of polymer particles. To coat MXene nanosheets on polymer particles, charged polymer particles and electrostatic interactions are usually used. Fusion of polymer particles into a monolithic film commonly involves heat, which might induce oxidation of MXenes.

Electrostatic attraction is usually used to assemble negatively charged MXene nanosheets on the surface of polymer particles, such as positively charged PS particles [93,94], positively charged polycarbonate particles [95], and positively charged PVDF particles [96]. For example, Sun et al. fabricated segregated "honeycomb-like" $Ti_3C_2T_z$/modified PS films for outstanding EMI shielding applications [93]. As is illustrated in Fig. 5**a**, dimethylaminomethacrylate methylchloride modified PS spherical particles (i.e., positively charged) were used as templates and mixed with an aqueous dispersion of $Ti_3C_2T_z$; electrostatic attraction between PS and nanosheets led to the coating of $Ti_3C_2T_z$ on PS spheres (SEM in Fig. 5**a**). Compression molding of the dried coated particles led to the formation of segregated $Ti_3C_2T_z$/PS films, where the nanosheets were distributed at the boundary of original PS spheres, as indicated in the cross-section TEM images of the films (Fig. 5**a**). The $Ti_3C_2T_z$ network within the PS matrix created effective electrically conductive pathways, yielding a superior electrical conductivity even at low filler loading (1081 S/m with only 1.9 vol% of $Ti_3C_2T_z$) compared to the homogenous counterparts made via solution mixing (2.2×10^{-7} S/m with 1.90 vol% of $Ti_3C_2T_z$). The architected composite gave high performance in EMI shielding (61.2 dB for 2 mm film), and the high degree of $Ti_3C_2T_z$/PS interface and multiple internal reflection gave high absorption (54.7 dB).

Rather than electrostatic attraction and flocculation, Luo et al. utilized electrostatic repulsion between negatively charged NR and $Ti_3C_2T_z$ to create a stable suspension [39]. The subsequent filtration process removed the solvent, resulting in segregated $Ti_3C_2T_z$/NR films, shown in Fig. 5**b**. An interconnected $Ti_3C_2T_z$ network within the NR matrix was formed, which is demonstrated by TEM, SEM, and EDS images (Fig. 5**b**). Similar to abovementioned $Ti_3C_2T_z$/PS film, the segregated $Ti_3C_2T_z$ network in NR matrix endowed the film with high electrical properties (1400 S/m and an outstanding EMI shielding performance of 53.6 dB with 6.71 vol% of MXene for a thin film of 251 μm). However, this method created rougher surfaces compared to compression molding of MXene coated polymer particles. Similar strategies were applied to other polymer compositions, such as $Ti_3C_2T_z$/vulcanized NR [97], $Ti_3C_2T_z$/PS [98], $Ti_3C_2T_z$/poly(methyl methacrylate) (PMMA) [99], and serine–modified $Ti_3C_2T_z$/serine modified epoxidized NR [100].

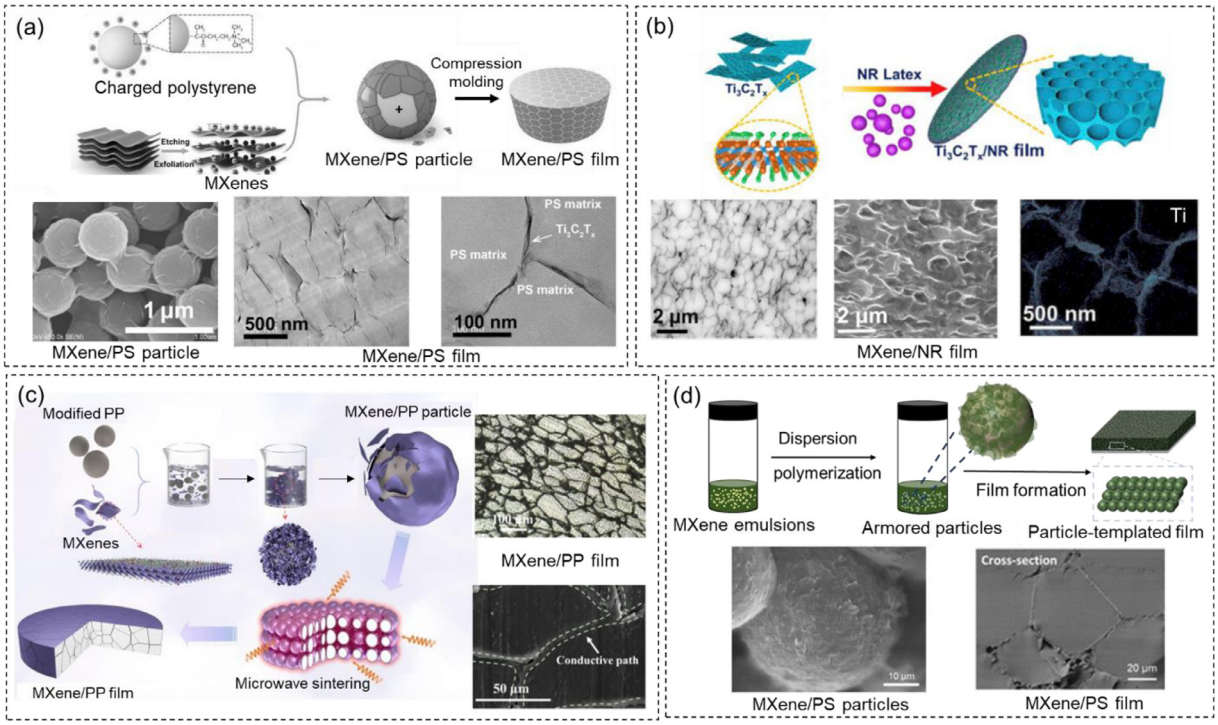

Fig. 5. MXene/polymer composite films prepared using the particle processing method and their corresponding segregated structures. (a) $Ti_3C_2T_z$/modified PS composite film via electrostatic assembly of positively charged PS and $Ti_3C_2T_z$ nanosheets, followed by compression molding. SEM and TEM images of the $Ti_3C_2T_z$-coated PS particle and cross-section of segregated $Ti_3C_2T_z$/modified PS film [93]. *Copyright 2017. Adapted with permission from John Wiley & Sons Inc.* (b) $Ti_3C_2T_z$/NR composite film via VAF of negatively charged NR with $Ti_3C_2T_z$ nanosheets and the SEM and EDS mapping (Ti) of the segregated film [39]. *Copyright 2019. Adapted with permission from Elsevier Science Ltd.* (c) $Ti_3C_2T_z$/modified PP composite film fabricated through microwave sintering of $Ti_3C_2T_z$-coated PP (positively charged) particles and optical and SEM images of the segregated structure [101]. *Copyright 2021. Adapted with permission from Elsevier Science Ltd.* (d) $Ti_3C_2T_z$/polymer (PS or polymethacrylate) composite film via in situ polymerization of $Ti_3C_2T_z$ stabilized monomer-in-water emulsions. SEM images show the $Ti_3C_2T_z$-coated PS particle and the cross-sectional $Ti_3C_2T_z$/PS film prepared by compression molding [105]. *Copyright 2021. Adapted with permission from American Chemical Society.*

The high heating response of MXene nanosheets to microwave irradiation enables the fabrication of segregated films from MXene-coated polymer particles and microwave irradiation. Ma et al. reported the microwave-assisted sintering of $Ti_3C_2T_z$/PP particles;[101] the particle feedstock was assembled by electrostatic attraction of positively charged PP and negatively charged $Ti_3C_2T_z$ nanosheets and the composite particles underwent selective heating when exposed to a microwave field, welding the PP granules together. As shown in the Fig. 5**c**, sintering yielded segregated $Ti_3C_2T_z$/PP composite films with a continuous and compact MXene network. The compacted $Ti_3C_2T_z$ network not only significantly enhanced the EMI shielding properties at low $Ti_3C_2T_z$ loading (>75 dB with 1.138 vol% of $Ti_3C_2T_z$ for a 2 mm film), but also improved the anti-dripping of PP due to the strong $Ti_3C_2T_z$ barrier effects. Similarly, other segregated polymer composites (such as CNT/polyetherimide composites) also employed the particle template processing and microwave sintering method [102].

In addition to ex situ mixing of polymer particles with MXene nanosheets, a recently developed emulsion-assisted assembly and in situ polymerization method can be used to produce MXene/coated polymer particles. This approach significantly expands the types of polymer particles that can be used to include neutral hydrophobic polymers, e.g., not cationic or anionic. The emulsion-assisted assembly involves the formation of emulsion droplets stabilized by MXene nanosheets, followed by polymerization of the droplets to form polymer particles with the MXene nanosheets coated on the surface. Bian et al. developed dodecane-in-water emulsions stabilized by $Ti_3C_2T_z$ nanosheets and cetyltrimethylammonium bromide, and subsequent freeze drying of the concentrated emulsions led to the formation of porous MXene aerogels [103]. Similarly, Shi et al. reported water-in-toluene emulsions stabilized by $Ti_3C_2T_z$ nanosheet and co-surfactants for structural liquids by jamming $Ti_3C_2T_z$ and amine-functionalized polyhedral oligomeric silsesquioxane at liquid-liquid interfaces and converstion to aerogels by freeze drying the concentrated emulsions [104]. More recently, Cao et al. reported monomer-in-water emulsions stabilized by salt-flocculated $Ti_3C_2T_z$ nanosheets to prepare $Ti_3C_2T_z$-coated polymer particles of PS and different polymethacrylates (Fig. 5**d**) [105]. As seen in the SEM image in Fig. 5**d,** the armored particles had a rough surface due to the coating and stacking of $Ti_3C_2T_z$ nanosheets. Compression molding above the T_g of the polymer particle created segregated $Ti_3C_2T_z$/PS films with an interconnected $Ti_3C_2T_z$ network along the particle boundaries, as shown in the cross-sectional SEM image. The composite film exhibited high absorption of radio frequency *(RF)* for heating (13−15 °C/s) in the range of 135−150 MHz and efficient EMI shielding of ~21 dB at low loading of $Ti_3C_2T_z$ of 1.2 wt%. Notably, homogeneous composites, i.e., with the organized MXene nanosheets, could not be prepared due to the orthogonal processing conditions of the nanosheets and polymer (e.g., no common solvent for solution casting and oxidation of MXenes under common melt processing conditions).

2.4. Polymer impregnation

Polymer impregnation can be used to fabricate networked MXene/polymer composites and involves the combination of bulk polymer with an already produced networked MXene structure. Usually, a 3D free-standing MXene skeleton is first fabricated (by methods such as freeze drying); then, liquid polymers are backfilled, followed by polymer solidification. Thus, a known MXene network is present within the polymer matrix, providing a perco-

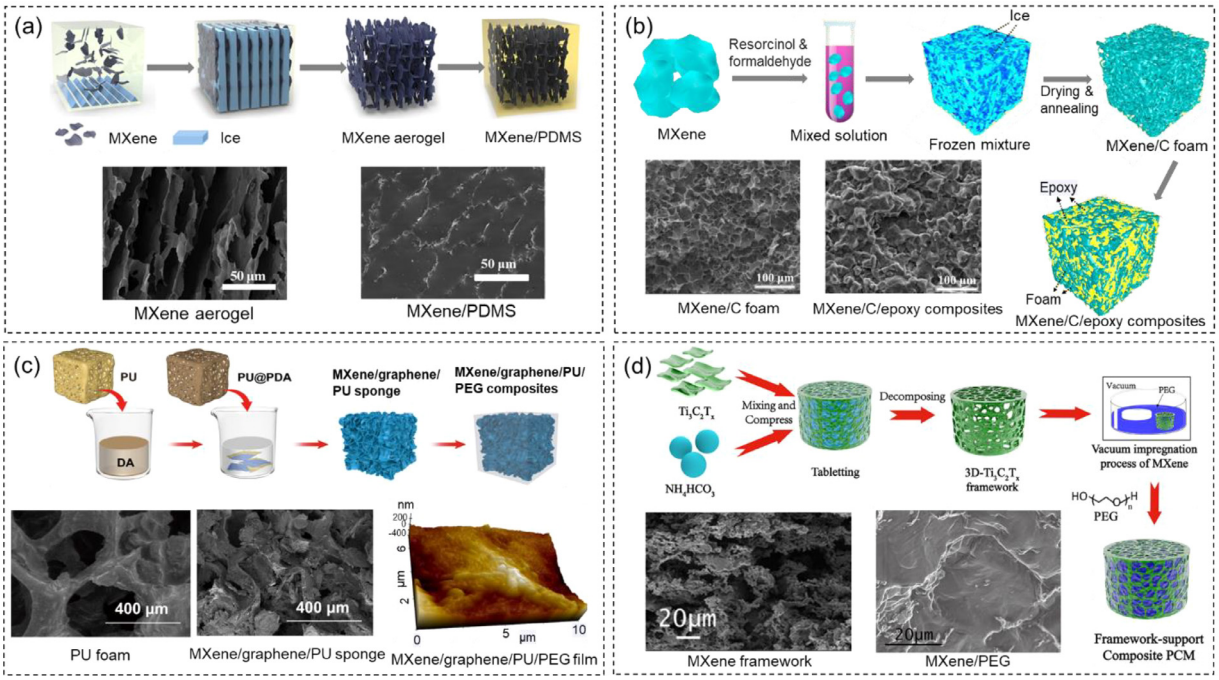

Fig. 6. MXene/polymer composite films prepared by polymer impregnation and their corresponding structures. (a) $Ti_3C_2T_z$/PDMS composite fabricated by impregnating PDMS into a porous $Ti_3C_2T_z$ skeleton (freeze dried), and SEM images showing porous $Ti_3C_2T_z$ aerogel skeleton and the impregnated $Ti_3C_2T_z$/PDMS film [106]. *Copyright 2020. Adapted with permission from Elsevier Science Ltd.* (b) $Ti_3C_2T_z$/C/epoxy composites prepared via polymer impregnation of epoxy into a porous $Ti_3C_2T_z$/C foam and their corresponding SEM images (left: $Ti_3C_2T_z$/C foam; right: $Ti_3C_2T_z$/C/epoxy film) [108]. *Copyright 2019. Adapted with permission from Elsevier Science Ltd.* (c) Fabrication of $Ti_3C_2T_z$/graphene-coated PU sponge and $Ti_3C_2T_z$/graphene/PU/PEG composite film via impregnation of PEG into the $Ti_3C_2T_z$/graphene/PU sponge. SEM images (from left to right) show the PU foam, $Ti_3C_2T_z$/graphene-coated PU foam, and $Ti_3C_2T_z$/graphene/PU/PEG film [114]. *Copyright 2022. Adapted with permission from Springer Nature Limited.* (d) Fabrication of $Ti_3C_2T_z$ skeleton using NH_4HCO_3 as a spatially confining agent and subsequent film formation via PEG impregnation. SEM images show the $Ti_3C_2T_z$ framework after removing NH_4HCO_3, and the $Ti_3C_2T_z$/PEG composite film [116]. *Copyright 2022. Adapted with permission from American Chemical Society.*

lated pathway, and the polymer coating provides mechanical support as well as oxidation stability for MXenes. The MXene network can be versatile in composition depending on the design and assembly methods. One challenge is that a large amount of MXene is needed to form an initial network. Another challenge is that suitable wetting of the MXene with the polymer is needed, thus limiting the use of hydrophobic polymers. Notably, Han *et al.* recently provided an excellent review on the assembly strategies of 3D MXene skeletons, and thus will not be addressed here [45].

Wang et al. fabricated $Ti_3C_2T_z$/PDMS composites by impregnating PDMS into freestanding $Ti_3C_2T_z$ aerogels, as is shown in Fig. 6**a** [106]. The $Ti_3C_2T_z$ aerogel was fabricated though a directional freeze drying method; here, only one side of the aqueous, highly concentrated MXene dispersion was placed in contact with the cold source and as the ice aligned upon formation the $Ti_3C_2T_z$ nanosheets assembled into an interconnected architecture (indicated by SEM in Fig. 6**a**). Then the $Ti_3C_2T_z$/PDMS composites were prepared by vacuum-assisted filling of PDMS prepolymer into the $Ti_3C_2T_z$ skeleton aerogel, followed by curing of PDMS at 100 °C. SEM images in Fig. 6**a** reveal that the pores were well-filled with PDMS, which gives good mechanical support and flexibility. The architected $Ti_3C_2T_z$/PDMS composites also benefited from the continuous $Ti_3C_2T_z$ network, resulting in high electrical conductivity (550 S/m with only 2.5 vol% of $Ti_3C_2T_z$) and thermal conductivity (2 times larger than pure PDMS), relevant to triboelectric nanogenerator applications. Yang et al. used a similar approach to prepare $Ti_3C_2T_z$/epoxy films by epoxy impregnation and the unique structural design showed promise for excellent Joule heating (reaching a steady-state temperature of 123 °C with a low voltage of 2 V and current of 5.1 A) [107].

Free-standing MXene-only skeletons usually suffer from poor mechanical properties and weak interactions between nanosheets, such that the structure may collapse because of the capillary forces during the polymer impregnation process. Researchers have developed MXene composite skeletons by introducing crosslinking agents to bind MXene nanosheets. For example, Wang et al. used resorcinol and formaldehyde with $Ti_3C_2T_z$ to form a composite skeleton [108]. The organic precursors tended to polymerize on the hydrophilic $Ti_3C_2T_z$ to connect the individual nanosheets and from a crosslinked $Ti_3C_2T_z$/C (thermally reduced) foam skeleton after polymer pyrolysis. As shown in the left SEM in Fig. 6**b**, the $Ti_3C_2T_z$/C composite skeleton had a well-connected structure with good mechanical properties (could support 500 times its own weight). Utilizing a similar polymer impregnation method of epoxy precursors and curing agents, a compact $Ti_3C_2T_z$/C/epoxy film structure was obtained (right SEM in Fig. 6**b**). With the benefit of the conductive inner network, the $Ti_3C_2T_z$/C/epoxy film exhibited high EMI shielding properties (46 dB with 1.64 wt% of $Ti_3C_2T_z$ and 2.61 wt% of C in a 2 mm thick composite film). The $Ti_3C_2T_z$/C skeleton also created multiple interfaces, enhancing multiple reflection and reabsorption, resulting in an absorption dominated EMI shielding mechanism (~39 dB for absorption). Other compositions of MXene skeleton have been prepared by using a similar approach; these include $Ti_3C_2T_z$/CNF [109-111], $Ti_3C_2T_z$/rGO/CNT [112], and $Ti_3C_2T_z$/MoS_2/CNF [113].

Another strategy for fabricating a strong robust MXene skeleton is by coating MXene on a porous polymer template. For example, Jin et al. reported the dip-coating of $Ti_3C_2T_z$ and graphene nanosheets on a modified polyurethane (PU) sponge (Fig. 6**c**) [114]. The porous PU sponge was first treated with polydopamine to enhance hydrophilicity, enabling it to be coated with $Ti_3C_2T_z$ and graphene, as shown in the SEM of a porous, rough $Ti_3C_2T_z$/graphene/PU structure in Fig. 6**c**. The PU sponge endowed the $Ti_3C_2T_z$/graphene/PU skeleton high flexibility and excellent

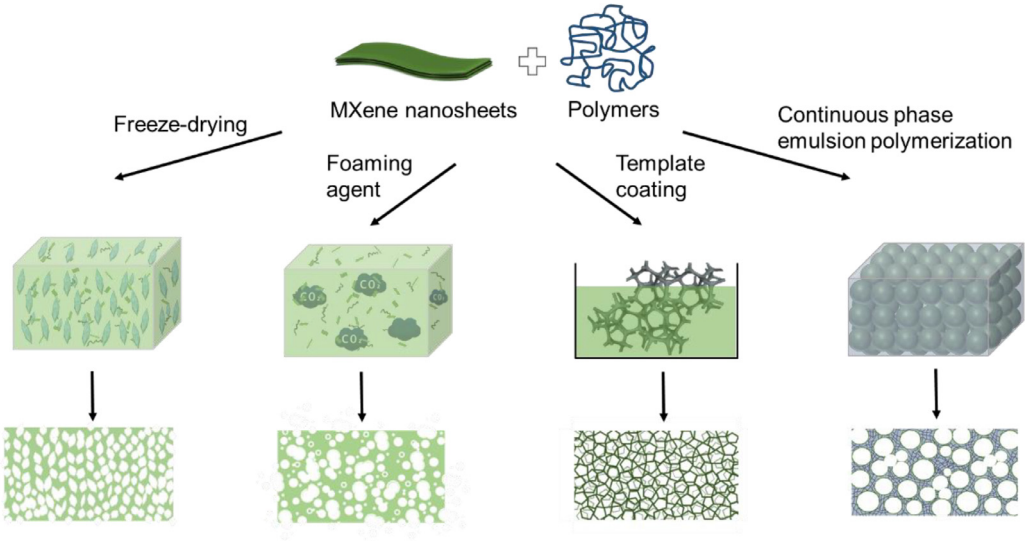

Fig. 7. Summary of the fabrication methods for structured MXene/polymer foams. Freeze casting involves the freezing of liquid MXene/polymer composites, then subsequent drying removes the ice by sublimation, leaving the pores in the solid composites. Foaming agents generate gaseous species which create pores. Template coating uses porous polymers as substrates for the coating of MXene nanosheets. Emulsion polymerization in the continuous phase and subsequent removal of the internal phase creates a MXene-coated porous polymer structure.

compressibility, which served as the strong inner network when forming a compact composite with polyethylene glycol (PEG) at 75 °C. The $Ti_3C_2T_z$/graphene/PU/PEG composites exhibited efficient EMI shielding properties (43.3 dB for 18.7 wt% of $Ti_3C_2T_z$ and graphene for a 2.4 mm film). Similarly, Shao et al. used melamine foam as a skeleton to produce flexible $Ti_3C_2T_z$/melamine/PEG composites for solar-thermal energy conversion [115].

To condense the MXene skeleton without significant changes in structure or collapse, a spatially confined forced network assembly method was developed. Chen et al. introduced NH_4HCO_3 as the spatial confining reagent to $Ti_3C_2T_z$ powder by grinding, and then formed a free-standing structure by mold pressing. After removing the NH_4HCO_3 in a hot vacuum oven, a dense, structurally stable $Ti_3C_2T_z$ skeleton was obtained, as is shown in Fig. 6**d**. By impregnating with molten PEG, a compact and void-free $Ti_3C_2T_z$/PEG composite structure was obtained (middle SEM in Fig. 6**d**). The compressed $Ti_3C_2T_z$ skeleton provided percolated thermal conduction pathway within the polymer matrix, leading to significant enhancements of thermal conductivity (10 times higher than pure PEG with 40 wt% $Ti_3C_2T_z$). The $Ti_3C_2T_z$/PEG composites exhibited rapid heating under sunlight irradiation for highly efficient photothermal conversion applications [116].

3. Foams

In complement to MXene/polymer films which are compact structures, and commonly free of voids, MXene/polymer foams are attractive due to their high flexibility, high surface area, low density, electrical conductivity, and absorption-favored electromagnetic properties [117,118]. As illustrated in Fig. 7, MXene/polymer foams are commonly fabricated through freeze drying, utilizing foaming agents, template coating, and emulsion polymerization. For example, freeze casting involves the freezing of liquid MXene/polymer composites, then the ice is removed under reduced pressure by sublimation, leaving pores in the solid composites. Similarly, foaming agents are used for pore generation during polymerization to fabricate MXene/polymer foams with controllable pore density. Template coating involves the use of a porous template (e.g., commercial foam) and the coating of MXenes forms a porous MXene/polymer foam structure. Polymerization in the continuous phase of an emulsion utilizing MXene as particle surfactants, followed by drying, immobilizes MXene nanosheets at the pore surfaces. The detailed corresponding characteristic structures for these methods will be discussed in the following subsections.

3.1. Freeze drying

Freeze drying is a relatively simple method for producing highly porous MXene/polymer structures with an interconnected network of nanosheets. First, an aqueous solution of polymer and MXenes is frozen, then the ice is removed by sublimation, leaving behind pores within the MXene/polymer composites. This method can introduce numerous pores, thus giving a low density structure, and the enlarged interface with air results in enhanced electromagnetic absorption and attenuation [51]. Further, directional freeze drying (with only one side the sample contacting with the cold source) can give controlled distribution and orientation of pores, producing anisotropic structures with favored pore alignments [119]. As freeze drying requires mixing of MXenes and polymers, this method is most commonly used with water dispersible, hydrophilic polymers. Notably, highly concentrated MXene nanosheets are needed for a robust and interconnected conductive network to form during freeze drying.

As a typical example of freeze drying to produce MXene/polymer foam, Xu et al. prepared highly porous MXene/PVA foam by freeze drying an aqueous mixture of concentrated Ti_2CT_z (30 mg/ml) and PVA [120]. As is illustrated in Fig. 8**a**, a lightweight Ti_2CT_z/PVA foam could stand upon a dandelion and contained macropores ~90 μm in diameter (SEM in Fig. 8**a**). Benefiting from the increased surface i.e., interface between composite and air), the Ti_2CT_z/PVA foam exhibited excellent EMI shielding properties (28 dB for 5 mm thick composite foam) with high absorption (26 dB), likely promoted by multiple internal reflection between the abundant air/composite interfaces. The authors verified this by compressing the Ti_2CT_z/PVA foam to eliminate the pores and observed a dramatic decrease of absorption (proportion of absorption decreasing from 0.59 to 0.04). In a similar vein, Xie *et al.* fabricated a $Ti_3C_2T_z$/CNF/Ni composite foam through freeze drying of cyclohexane-in-water emulsions, which were stabilized by the mixture of $Ti_3C_2T_z$, CNF, and Ni particles, and the pore size was dictated by emulsion droplet size [121]. This highly porous structure also had enhanced the multiple reflection and thus good ab-

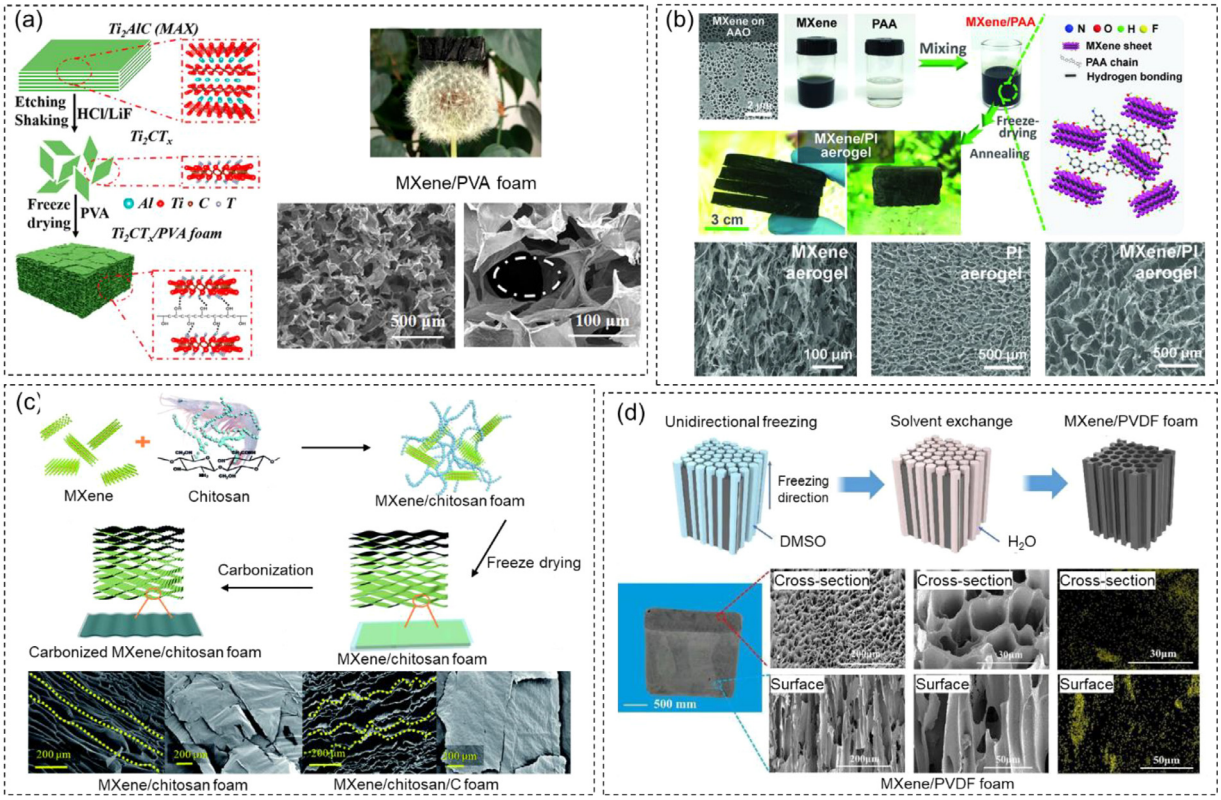

Fig. 8. MXene/polymer foam prepared by freeze drying. (a) Ti_2CT_z/PVA foam using freeze drying of a solution of Ti_2CT_z nanosheets and PVA. A digital image of dark foam showed the low density feature of Ti_2CT_z/PVA foam, which could stand on a dandelion. SEM images showed the Ti_2CT_z/foam at two different magnifications [120]. *Copyright 2019. Adapted with permission from American Chemical Society.* (b) Fabrication of $Ti_3C_2T_z$/PI aerogel using freeze drying and thermal annealing. SEM images (from left to right) show $Ti_3C_2T_z$ aerogel, PI aerogel, and $Ti_3C_2T_z$/PI composite aerogel [122]. *Copyright 2018. Adapted with permission from John Wiley & Sons Inc.* (c) $Ti_3C_2T_z$/chitosan foam and carbonized $Ti_3C_2T_z$/chitosan/C foam prepared by freeze drying and corresponding SEM images (side and top view) [123]. *Copyright 2019. Adapted with permission from the Royal Society of Chemistry.* (d) $Ti_3C_2T_z$/PVDF foam prepared by directional freeze drying. SEM and EDS mapping (Ti) of the cross-section and surface of the $Ti_3C_2T_z$/PVDF composite foam [124]. *Copyright 2022. Adapted with permission from Elsevier Science Ltd.*

sorption for EMI shielding applications (minimum refection loss of −30.2 dB for a 5 mm thick foam at 2.8 GHz).

To increase the flexibility and mechanical stability of MXene/polymer foam, strong interactions between MXene nanosheets and polymers need to be established. Liu et al. used polyimide (PI) to bridge $Ti_3C_2T_z$ nanosheets, forming a freestanding $Ti_3C_2T_z$/PI foam with excellent compressibility and stretchability by freeze drying of $Ti_3C_2T_z$/poly(amic acid) (PAmA) and subsequent polymerization (Fig. 8**b**) [122]. As shown in Fig. 8**b**, an aqueous solution of hydrophilic PAmA and $Ti_3C_2T_z$ was freeze dried then thermally annealed to induce polymerization of PAmA to PI. The strong polar interaction between PI and $Ti_3C_2T_z$ bound the two components together. As a result, the as-prepared $Ti_3C_2T_z$/PI foam was mechanically strong and could undergo compression, torsion, and even 180° bending. The SEM images (Fig. 8**b**) indicated a disordered structure for a pure $Ti_3C_2T_z$ aerogel, but the freeze dried $Ti_3C_2T_z$/PI foam exhibited a compact interface and interconnected porous structure. More importantly, the highly interconnected $Ti_3C_2T_z$ network endowed the composite foam with an electrical conductivity of 4 S/m with only ~0.084 vol% of $Ti_3C_2T_z$. In a similar vein, Hu and coauthors introduced protonated chitosan into an aqueous $Ti_3C_2T_z$ dispersion, followed by freeze drying and thermal annealing to fabricate $Ti_3C_2T_z$/chitosan/C foam, shown schematically in Fig. 8**c** [123]. The protonated chitosan has strong electrosatic interactions with negative $Ti_3C_2T_z$ nanosheets, such that chitosan provided a strong and continuous linkage between MXene nanosheets, resulting in enhanced compressibility and elasticity. The SEM in Fig. 8**c** shows the side and top view of the $Ti_3C_2T_z$/chitosan and $Ti_3C_2T_z$/chitosan/C foam, revealing the impact of annealing. Benefiting from the strongly connected $Ti_3C_2T_z$/chitosan/C structure and conductivity, the composite exhibited high sensitivity for pressure/strain sensors and wearable devices.

During the freezing process, ice growth can be regulated and pore orientation realized, thus resulting in anisotropic structures. For example, Han et al. fabricated a $Ti_3C_2T_z$/PVDF foam with aligned pores using a unidirectional freeze-solvent exchange-drying method [124]. As is shown in Fig. 8**d**, $Ti_3C_2T_z$ and PVDF were first mixed in DMSO, and the mixture was frozen by placing only the bottom of the container on the cold source. The frozen mixture was then washed with water at 4 °C (below the freezing point of DMSO) and oven dried at 30 °C to remove remaining DMSO and solidify PVDF. The SEM images and EDS mapping of Ti of the cross-section and surface of the $Ti_3C_2T_z$/PVDF foam indicate vertically aligned pores and the uniform distribution of $Ti_3C_2T_z$ in the pore walls (Fig. 8**d**). This unique anisotropic $Ti_3C_2T_z$/PVDF structure led to significant deformation differences based on orientation directions, which resulted in anisotropic sensing properties. For example, the foam could undergo larger deformation by application of force perpendicular to the pore channels compared to the parallel direction, resulting in higher pressure sensitivity (4 times higher). Anisotropic properties were also observed for a $Ti_3C_2T_z$/chitosan foam prepared using a similar directional freeze drying method, with superior compression stability when applying stress perpendicular to pore channels or lamellar layers compared to parallel [123].

3.2. Foaming agents

Gas foaming agents can also be used to create porous structures in MXene composites [125], though this approach is not as fully

explored as other methods. To use foaming agents, a MXene-based film is first prepared (e.g., by VAF) and then liquid foaming agents are introduced to treat the film, with the gas generated during this process creating numerous small pores. For example, Liu et al. reported the use of hydrazine to treat pure $Ti_3C_2T_z$ buckypapers; heating (90 °C) accelerated the reaction of hydrazine with -OH on the $Ti_3C_2T_z$ surface, generating large amounts of gasses, such as CO_2 and O_2 [126]. The gas species increased the volume between $Ti_3C_2T_z$ layers, and formed small pores in the pure $Ti_3C_2T_z$ structure. This process could easily produce large numbers of pores in the structure, but the precise control of the pore sizes was difficult. In another example, Su et al. leveraged hydrazine-induced foaming to fabricate porous $Ti_3C_2T_z$/CNF composites [127]. First, a $Ti_3C_2T_z$/CNF film was first prepared by VAF, then the film was put into an autoclave with 80 μL hydrazine monohydrate (80 wt%) and thermal treatment (90 °C) led to the rapid evolution of hydrazine hydrate vapor. The introduction of hydrazine and generated gasses expanded the layer spacing of the composite film, forming a porous structure. More importantly, hydrazine also provided a reductive environment, protecting MXenes for potential oxidation. The $Ti_3C_2T_z$/CNF foam exhibited high sensitivity for a wide range of pressures (419.7 kPa^{-1} for 0–8.04 kPa and 649.3 kPa^{-1} for 8.04–20.55 kPa). The hydrazine foaming technique has been used for other composite compositions, such as $Ti_3C_2T_z$/cellulose/layer double hydroxide [128], $Ti_3C_2T_z$/PANI [129], $Ti_3C_2T_z$/Ni/rGO/melamine [130]. Alternatively, supercritical CO_2 can be utilized to generate pores in MXene-based polymer composites. For example, Li et al. prepared $Ti_3C_2T_z$/CNT/PVDF foam by applying supercritical CO_2 to a pre-formed composite film in an autoclave (13.8 MPa, ~170 °C). After quickly releasing the pressure, pores were generated due the transition of CO_2 from a supercritical fluid to gas [131]. Similarly, Dehghan and co-authors reported the fabrication of $Ti_3C_2T_z$/rGO/PP using a supercritical CO_2 foaming method in an autoclave (14 MPa, 145 °C), giving a porous structure with efficient EMI shielding performance (25 dB with 10 wt% $Ti_3C_2T_z$/rGO (2:1 wt%:wt%) for a 2 mm thick sample) [132].

3.3. Dip coating

Dip coating is a method for fabrication of porous MXene polymer composites where MXene is coated on a porous polymer substrate surface. Typically, a porous substrate is prepared or commercially obtained, immersed in a dispersion of MXenes, and then dried. Advantages of the dip-coating method include tunable, preprogramed porosity and internal surface area, as well as commercial availability of some foams. Additionally, dip-coating can be repeated multiple times on the same sample, giving increased thickness of the MXene coating. Dip-coating doesn't require high concentrations of MXenes or high volumes of solution. However, the hydrophilicity of MXenes generally requires the use of a hydrophilic polymer, and nanosheet solutions may be viscous, preventing formation of a uniform coating on the porous substrate.

Yue et al. reported the fabrication of $Ti_3C_2T_z$/melamine foam via dip coating [133]. A melamine sponge with 97% porosity was immersed in an aqueous solution of $Ti_3C_2T_z$ (0.5 mg/mL, 1 mg/mL, and 2 mg/mL), then dried for 24 h in a vacuum oven. The 3D network had a thin layer of $Ti_3C_2T_z$ on the surface of the sponge, as supported by the SEM image and EDS mapping shown in Fig. 9**a**. Strong van der Waals forces and the large surface area of $Ti_3C_2T_z$ allowed the nanosheets to be well coated on the substrate skeleton surface. The interconnected 3D network of $Ti_3C_2T_z$/melamine foam and good compressibility endowed the composite foam as a promising pressure sensor. The sensor used an electrode fabricated by assembling $Ti_3C_2T_z$ foam onto a predeposited PVA nanowire network andshowed high sensitivity over a broad pressure range (147 kPa^{-1} for less than 5.37 kPa and 442 kPa^{-1} for 5.37–18.56 kPa region). Additionally, this network showed conductivity values of 0.004 S/m without pressure on the foam. Another study used a similar melamine sponge and dip-coated the $Ti_3C_2T_z$ nanosheets not only on the skeleton of the polymer, but also the cells, forming a closed-cell structure of $Ti_3C_2T_z$/melamine composites. The continuous $Ti_3C_2T_z$ coating formed closed and conductive cells around the pores, which exhibited excellent EMI shielding values of 90.5 dB at 0.82 vol% loading for a 2 mm thick foam sample [134]. Similarly, Li et al. submerged a commercial PU sponge and in a 5 mg/mL solution of $Ti_3C_2T_z$ nanosheets to prepare $Ti_3C_2T_z$/PU composite foams [135]. The $Ti_3C_2T_z$ coating enhanced the anti-dripping properties, such that during the combustion process the sample maintained its original shape and no melt droplets were observed. Other MXene/polymer foams that have been prepared by dip coating include $Ti_3C_2T_z$/melamine/PEDOT:PSS [136], $Ti_3C_2T_z$/triaxially auxetic PU [137], $Ti_3C_2T_z$/PANI/PP [138], and $Ti_3C_2T_z$/melamine/PDMS [139].

Controlling the pore structure is an important element of composite foams. For dip-coating method, the pore structure is controlled by the porous substrate. For example, Li et al. used a salt template approach to synthesize a TPU foam with controlled pore structure [140]. The density and porosity of the foam was altered by changing the NaCl to TPU ratio, as indicated in Fig. 9**b**. Increasing the NaCl:TPU ratio from 5:1 to 9:1 decreased the density of the sample from 0.3836 g/cm^3 to 0.1960 g/cm^3 and increased the porosity from 61 % to 80 %. SEM showed rough stacking of $Ti_3C_2T_z$ nanosheets on the foam pores (Fig. 9**b**). Further, higher concentrations of NaCl led to better connected pores within the foam, which facilitated the formation of open cell voids. The foam had high flexibility and was able to be bent and twisted without permanent deformation. Electrical conductivity was compared across different porosities and $Ti_3C_2T_z$ loadings, and the sample with 74 % porosity and at 0.66 vol% of $Ti_3C_2T_z$ coating had highest electrical conductivity (290.8 S/m.) and good EMI shielding performance (72.2 dB for the 2 mm thick sample). To confirm the consistent EMI shielding performance under mechanical deformation, the $Ti_3C_2T_z$/TPU foams were compressed at 10 %, 30 %, and 50 % strain, and EMI shielding effectiveness only slightly decreased from 72.2 dB to 68.6 dB, which may be due to damage of the 3D network. Notably, treating the TPU with polydopamine (PDA) before coating with $Ti_3C_2T_z$ led to better adhesion of the nanosheets.

The dip-coating approach onto porous substrates can be integrated with an LbL approach to give a foam with layered coatings. Lin et al. coated a PU foam (negatively charged) with chitosan/$Ti_3C_2T_z$ multilayers by alternately dipping the PU foam in chitosan solution and then $Ti_3C_2T_z$ dispersion until the desired number of layers was achieved [141]. FTIR spectroscopy confirmed functionalization with weak characteristic adsorption bands of PU, suggesting that the coatings were compact on the PU surface, and an obvious C-F peak was supported deposition of $Ti_3C_2T_z$. SEM imaging revealed that the porous structure of the foam was maintained (Fig. 9**c**), and the PU foam showed only a 6.9 wt% gain. With increased number LbL deposition, the surface of the PU foam became rougher (see "zoom in" SEM image). The $Ti_3C_2T_z$/chitosan LbL coating significantly improved the fire-retardant properties (57.2 % reduction in the peak heat release). Alternatively, Tian et al. used a 3D Ni substrate and LbL dip coating with $Ti_3C_2T_z$ and polyethyleneimine to create a binder-free electrode for high performance supercapacitors (370 F/g at 2 mV/s scanning rate) [142]. Thus dip coating LbL assembly onto porous substrates allows for production of relatively well-defined and sometimes complicated structures [143–145].

An alternative to standard dip-coating approach is an "inside-out" method which produces a MXene 3D structure coated with

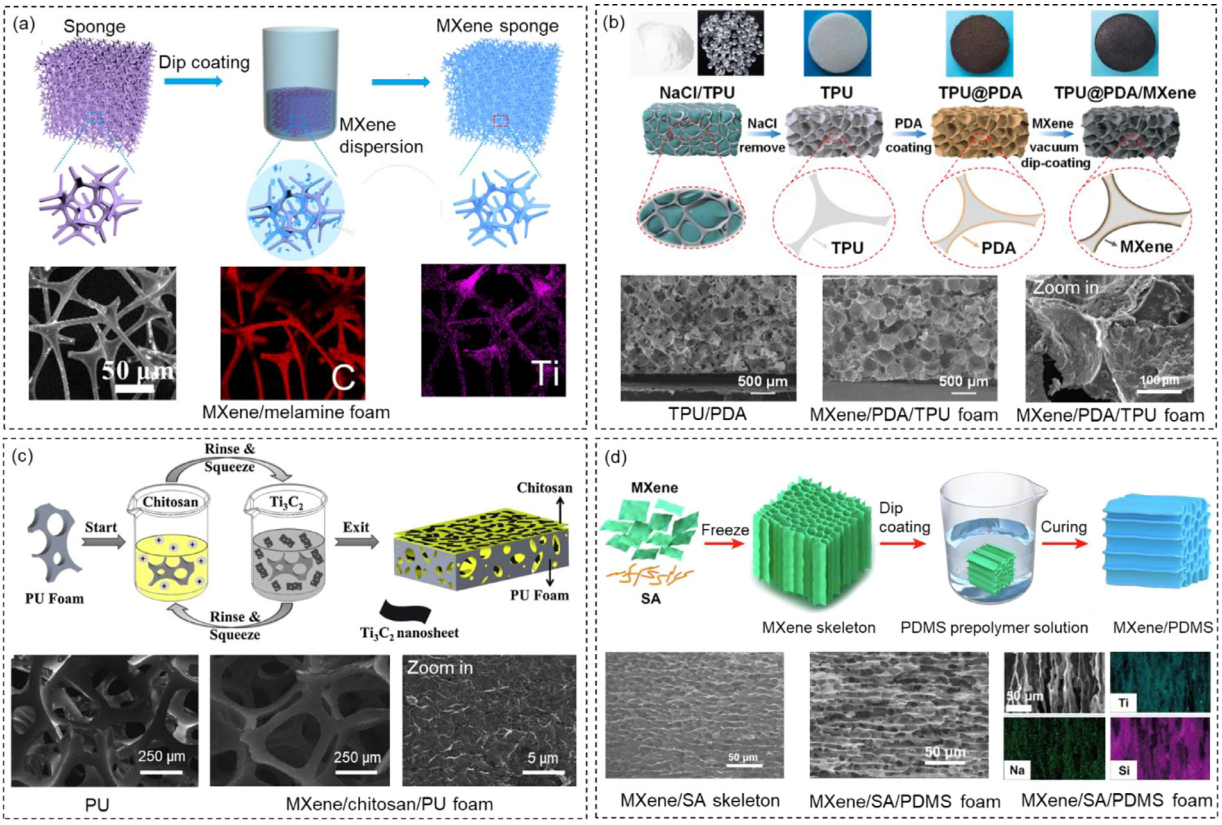

Fig. 9. MXene/polymer foams prepared via dip-coating. (a) $Ti_3C_2T_z$/melamine foam fabricated by dip-coating of $Ti_3C_2T_z$ nanosheets on commercial porous melamine substrate. SEM image shows the $Ti_3C_2T_z$/melamine foam and EDS mapping (C and Ti) indicate uniform coating of $Ti_3C_2T_z$ nanosheets [133]. *Copyright 2018. Adapted with permission from Elsevier Science Ltd.* (b) $Ti_3C_2T_z$/PDA/TPU foam fabricated by dip-coating of $Ti_3C_2T_z$ nanosheets on porous PDA/TPU foam. SEM images show the PDA/TPU foam before and after dip coating with $Ti_3C_2T_z$ nanosheets, and the zoomed in image shows the rough surface of $Ti_3C_2T_z$/PDA/TPU foam [140]. *Copyright 2023. Adapted with permission from Elsevier Science Ltd.* (c) $Ti_3C_2T_z$/chitosan/PU foam fabricated by alternating dip-coating of chitosan and $Ti_3C_2T_z$ nanosheets on PU foam. SEM images show a PU substrate before and after coating of multiple layers of $Ti_3C_2T_z$/chitosan, and rough surface morphology of the composite foam [141]. *Copyright 2020. Adapted with permission from Elsevier Science Ltd.* (d) $Ti_3C_2T_z$/SA/PDMS foam fabricated by dip-coating of PDMS polymer on porous $Ti_3C_2T_z$/SA skeleton (made by directional freeze drying). SEM images of $Ti_3C_2T_z$/SA skeleton and $Ti_3C_2T_z$/SA/PDMS foam, and EDS mapping (Ti, Na, and Si) of the $Ti_3C_2T_z$/SA/PDMS composite foam [146]. *Copyright 2020. Adapted with permission from Elsevier Science Ltd.*

polymer (rather than a polymer 3D structure coated with MXenes). Wu et al. fabricated a porous $Ti_3C_2T_z$ skeleton and then deposited polymer by dip-coating [146]. First, a $Ti_3C_2T_z$/SA aerogel was fabricated by directional freeze drying a $Ti_3C_2T_z$/SA suspension. The aerogel was dipped in a PDMS pre-polymer and cured at 60 °C to create a $Ti_3C_2T_z$/SA/PDMS foam. In contrast to polymer impregnation to form a compact bulk polymer around MXene skeleton, the dip-coating only forms a thin layer of polymer on the surface of the porous MXene skeleton. SEM imaging (Fig. 9**d**) shows the ordered porous $Ti_3C_2T_z$/SA aerogel before (left SEM image) and after the dip-coating of PDMS (middle SEM image), verifying that the pores did not collapse after the PDMS coating and curing. The polymer coating on the $Ti_3C_2T_z$/SA skeleton was confirmed by the EDS mapping of Si, Na, and Ti. The ordered channels formed a conductive network that facilitated charge carrier transport by reducing the interfacial resistance. The composite containing 6.1 wt% $Ti_3C_2T_z$ exhibited an EMI shielding effectiveness of 53.9 dB, significantly larger than a counterpart prepared by blending PDMS pre-polymer and $Ti_3C_2T_z$ powder (9.1 dB). The high EMI shielding properties of the architected $Ti_3C_2T_z$/SA/PDMS foam can be attributed to the well-connected network of $Ti_3C_2T_z$ nanosheets, whereas the PDMS coating provided high flexibility and mechanical robustness, allowing for repeated compression (>500 times).

3.4. Emulsion polymerization

A simple way to create porous polymer nanocomposites is to use nanoparticles (such as GO, cellulose, MXenes) as Pickering surfactants in an emulsion, coupled with polymerization selectively in the continuous phase. This method provides an alternative strategy to fabricate segregated MXene/polymer foams with tunable porosity. Specifically, MXenes can act as solid particle surfactants (so-called Pickering surfactants) by their localization and assembly at the interface between the continuous and dispersed (i.e., droplet) phases of emulsions. In-situ polymerization of the continuous phase leads to the formation of polymer struts between droplets such that removal of dispersed phase leads to a porous structure lined with MXene nanosheets. Further, the pore size and distribution can be tailored by simply changing the surfactant concentration and/or dispersed phase content, giving access to open-cell or close-cell foams with the same composition [147,148]. A common challenge associated with the emulsion-templated method is the high hydrophilicity of MXenes, which limits the type of monomers that can be used in the continuous phase. Moreover, this approach sometimes requires the use of organic co-surfactants to drive MXenes to the interfaces, requiring their removal after processing.

Various Pickering emulsion systems have been used to organize MXenes, such as dodecane-in-water emulsions [103], water-in-toluene emulsions [104], and styrene-in-water emulsions [105]. Recently, Zheng et al. prepared $Ti_3C_2T_z$/polystyrene composite foam using water-in-styrene Pickering emulsions and polymerization [149]. As is shown in Fig. 10**a**, $Ti_3C_2T_z$ nanosheets were modified with hydrophobic molecules (dihexadecyldimethylammonium bromide) to enable them to serve as particle stabilizers for water-in-styrene emulsions. Highly concentrated emulsions were formed by employing a high content of internal phase, commonly re-

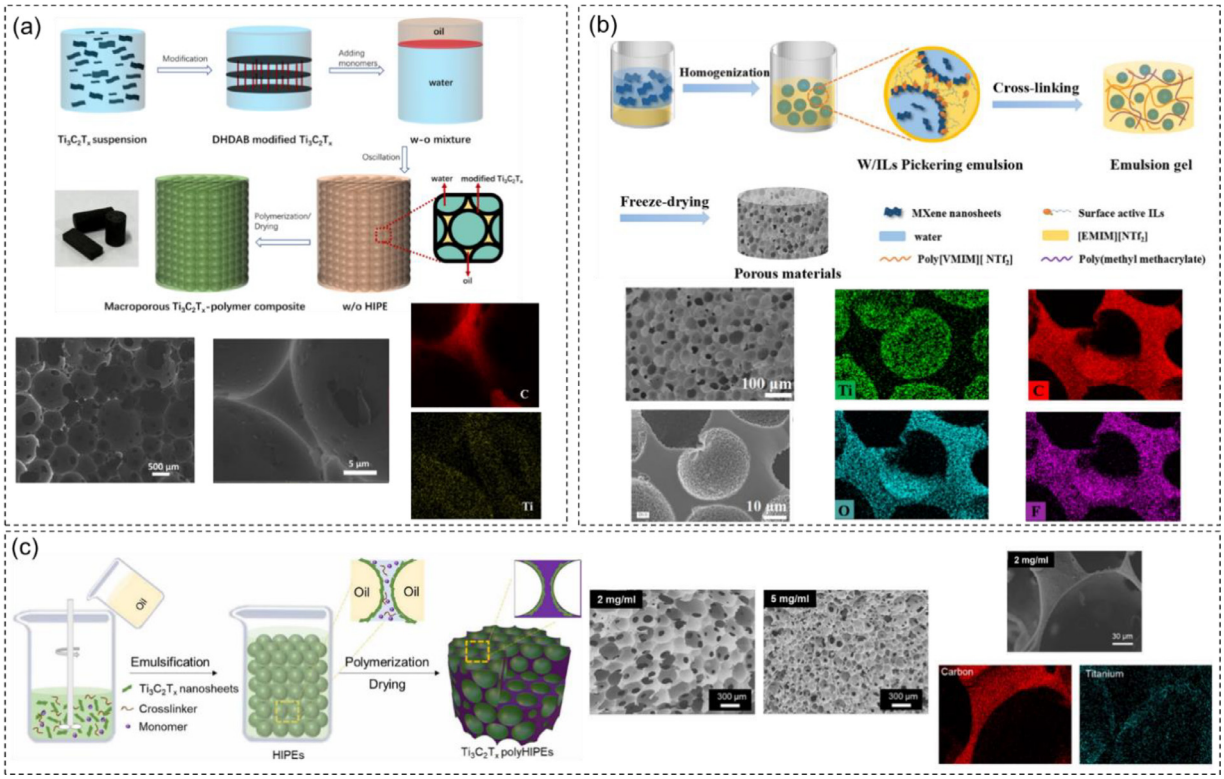

Fig. 10. MXene/polymer foams prepared via polymerization in the continuous phase of an emulsion. (a) $Ti_3C_2T_z$/PS polyHIPE foam fabricated from water-in-oil emulsions and SEM images and EDS mapping (C and Ti) of $Ti_3C_2T_z$/PS polyHIPEs [149]. *Copyright 2022. Adapted with permission from Elsevier Science Ltd.* (b) $Ti_3C_2T_z$/polyIL polyHIPE fabricated from water-in-IL emulsions and the corresponding SEM and EDS mapping (Ti, C, O, and F) of the polyHIPE structure [150]. *Copyright 2022. Adapted with permission from Elsevier Science Ltd.* (c) $Ti_3C_2T_z$/PAM polyHIPE fabricated from oil-in-water emulsion, SEM images of the polyHIPEs with different $Ti_3C_2T_z$ concentrations, and EDS mapping (C and Ti) of porous $Ti_3C_2T_z$/PAM polyHIPEs [151]. *Copyright 2022. Adapted with permission from IOP Publishing Ltd*.

ferred to high internal phase emulsions (HIPEs). By polymerizing styrene in the continuous phase and removing the internal water phase, a highly interconnected porous $Ti_3C_2T_z$/polystyrene foam was obtained (also referred to polyHIPEs, SEM in Fig. 10**a**). EDS mapping of the foam clearly showed the polymer strut and localization of $Ti_3C_2T_z$ on the surface of the pores, represented by the C (red) and Ti (yellow) dots respectively. The precise control of the $Ti_3C_2T_z$ nanosheet location allows for the construction of interconnected, conductive networks with low loading of $Ti_3C_2T_z$ (1.15 S/m for 0.090 vol% of $Ti_3C_2T_z$). Alternatively, Fan and coworkers used a water-in-ionic liquid (IL) emulsion system to form a $Ti_3C_2T_z$/polyIL composite foam [150]. Fig. 10**b** schematically shows the approach to using 3-hexadecyl-1-vinylimidazolium bromide-modified $Ti_3C_2T_z$ as the Pickering surfactants, and subsequent crosslinking and freeze drying led to porous composite foam. SEM images and EDS mapping support the localization of $Ti_3C_2T_z$ nanosheets on the pore surfaces, even in a closed-cell system. This unique distribution of $Ti_3C_2T_z$ nanosheets in the composites endowed the foam with good electrical properties and the composites could be applied as piezoresistive sensor with high sensitivity (2.285 kPa^{-1} vs. 17.411 kPa^{-1} at low (<5 kPa) and higher pressure regime (5–20 kPa), respectively).

More recently, a co-surfactant free method was developed to prepare MXene/polymer polyHIPEs. Cao et al. utilized common salt (e.g., NaCl) to partially flocculate an aqueous dispersion of $Ti_3C_2T_z$ nanosheets, which could then stabilize a dodecane-in-water HIPE. By loading the continuous phase with acrylamide, cross-linker, and initiator, thermally initiated polymerization yielded porous $Ti_3C_2T_z$/polyacrylamide composite foam (Fig. 10**c**) [151]. Again, distinct polymer struts and uniform $Ti_3C_2T_z$ nanosheet coating on the pore surfaces were supported by EDS mapping of C and Ti (Fig. 10**c**). Additionally, the pore size of the polyHIPE foam could be tuned; increasing the $Ti_3C_2T_z$ concentration led to decreased size of the emulsion droplets, and consequently, a decrease in the pore size of the composite foam (SEM images in Fig. 10**c**). Benefiting from the unique interconnected pores as well as the $Ti_3C_2T_z$ coating on the pores, the $Ti_3C_2T_z$/PAM polyHIPE foam exhibited rapid *RF* heating, even at low powers (10 °C/s at 1 W).

4. Outlook and conclusion

Despite the increasing number of studies that address architecting MXene/polymer composites, a number of challenges must be addressed to identify and leverage the potential of these materials for addressing societal needs. To date, most MXene/polymer composites focus on monolithic films and foams, leaving MXene/polymer capsules[152,153] and bicontinuous emulsions under explored [154]. For example, Cao and coworkers used MXene-stabilized emulsions and interfacial polymerization to produce MXene/polyurea capsules (Fig. 11**a**) [152]. This approach can be used to produce capsules filled with a core liquid of choice, such as salt hydrate phase change material or IL (e.g., for contaminant removal [155,156], thermal energy management [157], or CO_2 capture[158–160]). Alternatively, Wu et al. reported the fabrication of hollow $Ti_3C_2T_z$/hydroxyapatite (HAP)/chitosan/hyaluronic acid (HA) composite capsules using LbL assembly of HAP, chitosan/HA, and $Ti_3C_2T_z$ on sacrificial $CaCO_3$ particles (Fig. 11**b**); these capsules were used for pH/near infrared multi-responsive drug delivery applications [153]. In addition, Wang et al. reported the fabrication of $Ti_3C_2T_z$/GO/water/resin bijels from bicontinuous emulsions, with subsequent resin curing and water removal giving conductive foams with rapid RF heating [154]. These examples indicate the potential of MXenes to be incorporated into new structures for tailored applications. The processing-structure-property relationship

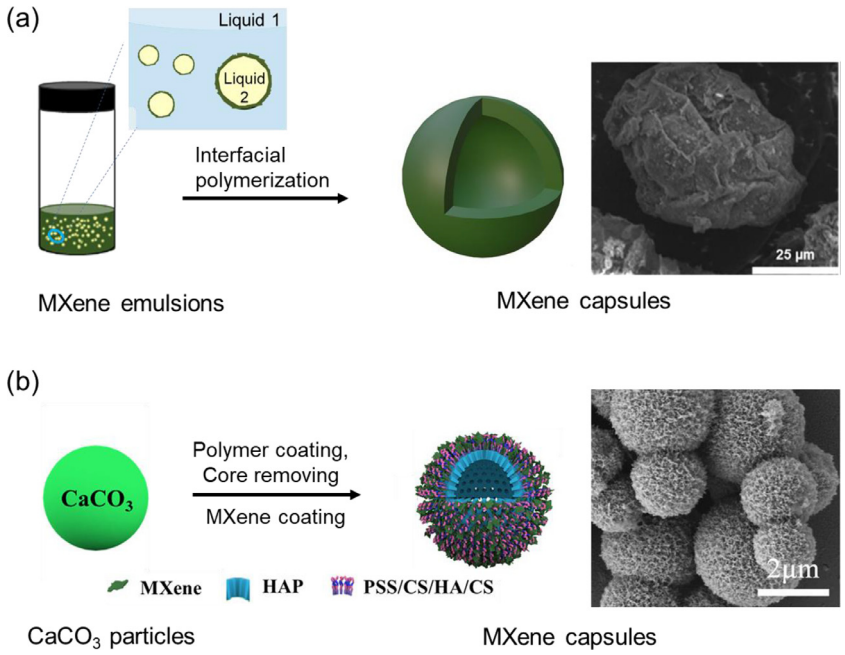

Fig. 11. Non-monolith MXene/polymer composites. (a) $Ti_3C_2T_z$/polyurea hollow capsules fabricated by emulsion templated interfacial polymerization and SEM images of the capsules [152]. *Copyright 2021. Adapted with permission from American Chemical Society.* (b) $Ti_3C_2T_z$/HAP/chitosan/HA capsules fabricated by LbL on a sacrificial $CaCO_3$ template particle and SEM images [153]. *Copyright 2021. Adapted with permission from Elsevier Science Ltd.*

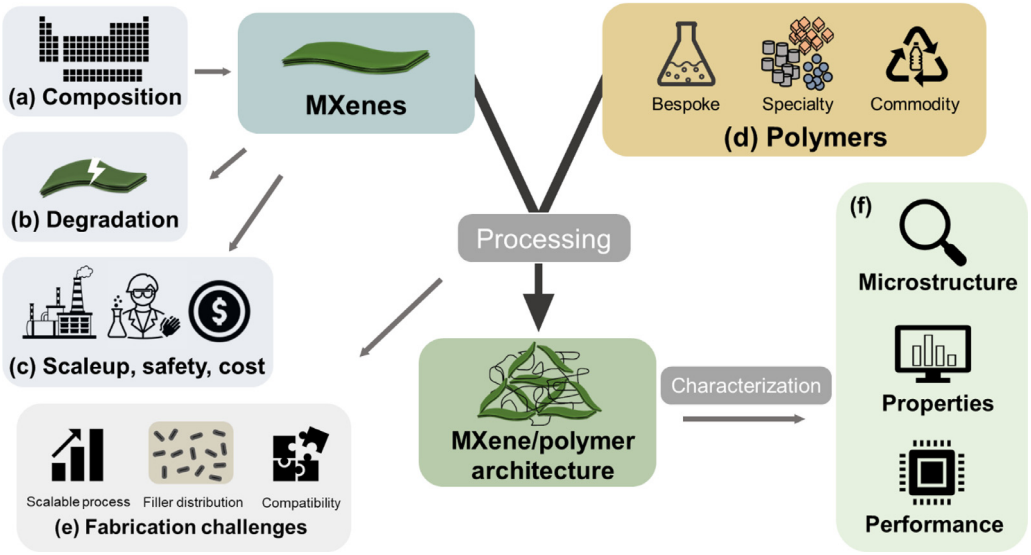

Fig. 12. Schematic of the current opportunities and challenges for structured MXene/polymer composites: The challenges for MXene production include (a) widening the range of possible MXene compositions, (b) mitigating the threat of MXene degradation, (c) scaling up MXene production in a safe and cost-effective manner. The next step is to process MXenes together with (d) commercially relevant polymers and address the (e) fabrication challenges described in this review, in concert with (f) multi-characterization of the result products.

of these MXene/polymer architectures is needed to deconvolute the composition and structure of MXene/polymer composites for certain properties relevant to advanced applications.

Additional challenges include the following. Most of the MXene/polymer composites use $Ti_3C_2T_z$ because of their relative ease of synthesis and stability; this leaves other MXene compositions less explored for polymer composites. Future work should address the versatility of structured MXene/polymer composites with different MXene compositions (e.g., V-based MXene, Nb-based MXenes, or nitrides) and explore their distinct properties (such as catalytic properties, Fig. 12**a**). MXenes also face the ongoing challenge of degradation stability (Fig. 12**b**), as the nanosheets can undergo oxidation or hydrolysis in aqueous and other oxygen-rich media. The use of water or other oxygen-rich media is thus a concern when processing MXene with polymers for a composite material, especially when oxidizing reagents are used, such as initiators for in situ polymerization. Efforts to minimize the degradation of MXenes during synthesis include the use of high-quality MAX phase[161] or a MAX phase with excess Al (e.g., Al-Ti_3AlC_2) [18]. After synthesis, low-temperature storage, the addition of antioxidants, or incorporation into a polymer can also help slow MXene degradation [162]. Moreover, different synthesis methods lead to varied lateral size distribution and varied number of layers; these geometric factors can greatly affect their incorporation into poly-

mer systems. Although most reports assume single layer MXene nanosheets are present in a stable colloidal dispersion, a detailed relationship of MXene size and their fabrication in polymer composites and resulting properties needs to be addressed.

MXene synthesis is still at lab scale (Fig. 12**c**), which limits the commercial feasibility and practicality of MXene/polymer composites. Progress will be directly tied to the development of scalable synthesis of MXenes in a safe (e.g., overcome the use of HF) and cost-effective way. For composite fabrication, off-the-shelf, commercially available polymers are most commonly used, though the varied polymer chemistries that are continually being developed can help to tune not only polymer-nanosheet interactions, but also final properties (Fig. 12**d**). Fabrication of MXene-polymer composites usually involves multiple steps and complicated procedures, particularly in maintaining control over the distribution of MXenes in polymer matrix at larger scales (Fig. 12**e**). Even though some polymers are commercially available for composites (such as commercial resins or foams), significant pre-processing (such as surface modification to functionalize the nanosheets or polymers) is needed for producing MXene/polymer composites due to differences in surface chemistry (Fig. 12**e**).

Lastly, multiple characterization techniques across different disciplines are essential to investigate and fuly characterize the structured MXene/polymer composites, including analyzing the chemical composition of MXenes and polymers, exploring their microscopic and macroscopic structures, evaluating properties (e.g., mechanical, thermal, and electrical), and assessing performance-related applications (Fig. 12**f**). Experts in 2D particles, polymers, characterization, manufacturing, and applications need to work together to establish standardized methodology and comprehensive understanding on architected MXene/polymer composites.

To conclude, we have herein summarized recent advances for the production of architected MXene/polymer composite films and foams, and the relationship of these tailored architectures to performance-related properties, when available. This highlights the potential superior properties of structured MXene/polymer composites for advanced applications, especially compared to non-structured, isotropic counterparts. We focus on the organization of MXenes within a polymer matrix for each method, highlighting the processing-structure relationship for design of new MXene/polymer systems. We discussed MXene/polymer films in Section 2, focusing on four common fabrication methods (vacuum-assisted filtration, layer-by-layer assembly, particle processing, and polymer impregnation) and their corresponding unique architectures in detail, including processing conditions, compositions, and filler distributions. In Section 3, we focused on porous MXene/polymer structures and their fabrication techniques, such as freeze drying, foaming agents, dip-coating, and emulsion polymerization. In addition to the processing-structure relationship, we also discuss the property improvements of MXene/polymer composites benefited from their unique structures for both films and foams, including electrical and thermal conductivity, EMI shielding effectiveness, capacitance, fire-retardant property, sensing property, and Joule and RF heating, indicating the potential of architected MXene/polymer composites for advanced applications. In Section 4, we discussed the current challenges and potential opportunities for addressing architected MXene/polymer composites, such as broadening the MXene compositions used, scaled up synthesis of MXenes, mitigating MXene degradation, using a variety of polymer chemistries, fabrication challenges, and multi-disciplinary characterization needs. Additionally, the processing and fabrication strategies for architected polymer composites discussed in this review can extend beyond MXenes to other nanoparticles, which provides valuable insight into exploring processing-structure-property relationships for architected nanomaterial/polymer composites.

Declaration of competing interest

The authors declare that they have no known competing financial interests or personal relationships that could have appeared to influence the work reported in this paper.

CRediT authorship contribution statement

Huaixuan Cao: Writing – review & editing, Writing – original draft, Visualization, Conceptualization. **Natalie N. Neal:** Writing – review & editing, Writing – original draft. **Savannah Pas:** Writing – review & editing, Writing – original draft. **Miladin Radovic:** Writing – review & editing. **Jodie L. Lutkenhaus:** Writing – review & editing. **Micah J. Green:** Writing – review & editing, Supervision, Project administration, Conceptualization. **Emily B. Pentzer:** Writing – review & editing, Project administration, Conceptualization.

Data availability

No data was used for the research described in the article.

Acknowledgments

The authors thank Texas A&M University for financial support. EP thanks NSF DMR award #2103182; MJG, JLL, and MR thanks NSF CMMI award #2240554. The authors also thank Kailash Arole and Vrushali Kotasthane of TAMU for helpful input.

References

[1] Deng H, Lin L, Ji M, Zhang S, Yang M, Fu Q. Progress on the morphological control of conductive network in conductive polymer composites and the use as electroactive multifunctional materials. Prog Polym Sci 2014;39:627–55.
[2] Aghamohammadi H, Amousa N, Eslami-Farsani R. Recent advances in developing the MXene/polymer nanocomposites with multiple properties: a review study. Synth Met 2021;273:116695.
[3] Chen H, Ginzburg VV, Yang J, Yang Y, Liu W, Huang Y, et al. Thermal conductivity of polymer-based composites: fundamentals and applications. Prog Polym Sci 2016;59:41–85.
[4] Gan PG, Sam ST, MFb Abdullah, Omar MF. Thermal properties of nanocellulose-reinforced composites: a review. J Appl Polym Sci 2020;137:48544.
[5] Shang L, Xu J, Nienhaus GU. Recent advances in synthesizing metal nanocluster-based nanocomposites for application in sensing, imaging and catalysis. Nano Today 2019;28:100767.
[6] Obisesan OS, TO Ajiboye, Mhlanga SD, Mufhandu HT. Biomedical applications of biodegradable polycaprolactone-functionalized magnetic iron oxides nanoparticles and their polymer nanocomposites. Colloids Surf B Biointerfaces 2023;227:113342.
[7] Li J, Liu X, Feng Y, Yin J. Recent progress in polymer/two-dimensional nanosheets composites with novel performances. Prog Polym Sci 2022;126:101505.
[8] Kuilla T, Bhadra S, Yao D, Kim NH, Bose S, Lee JH. Recent advances in graphene based polymer composites. Prog Polym Sci 2010;35:1350–75.
[9] Sun X, Huang C, Wang L, Liang L, Cheng Y, Fei W, et al. Recent progress in graphene/polymer nanocomposites. Adv Mater 2021;33:2001105.
[10] Baig N. Two-dimensional nanomaterials: a critical review of recent progress, properties, applications, and future directions. Compos Part A Appl Sci Manuf 2023;165:107362.
[11] Gogotsi Y, Anasori B. The rise of MXenes. ACS Nano 2019;13:8491–4.
[12] VahidMohammadi A, Rosen J, Gogotsi Y. The world of two-dimensional carbides and nitrides (MXenes). Science 2021;372:eabf1581.
[13] Gogotsi Y, Huang Q. MXenes: two-dimensional building blocks for future materials and devices. ACS Nano 2021;15:5775–80.
[14] Naguib M, Kurtoglu M, Presser V, Lu J, Niu J, Heon M, et al. Two-dimensional nanocrystals produced by exfoliation of Ti3AlC2. Adv Mater 2011;23:4248–53.
[15] Li M, Lu J, Luo K, Li Y, Chang K, Chen K, et al. Element Replacement Approach by Reaction with Lewis Acidic Molten Salts to Synthesize Nanolaminated MAX Phases and MXenes. J Am Chem Soc 2019;141:4730–7.
[16] Liu L, Orbay M, Luo S, Duluard S, Shao H, Harmel J, et al. Exfoliation and Delamination of Ti3C2Tx MXene Prepared via Molten Salt Etching Route. ACS Nano 2022;16:111–18.
[17] Wang F, Wang S, Tian F, Wang F, Xia X, Zhang Q, et al. Advances in molten-salt-assisted synthesis of 2D MXenes and their applications in electrochemical energy storage and conversion. Chem Eng J 2023;470:144185.
[18] Mathis TS, Maleski K, Goad A, Sarycheva A, Anayee M, Foucher AC, et al. Modified MAX Phase Synthesis for Environmentally Stable and Highly Conductive Ti3C2 MXene. ACS Nano 2021;15:6420–9.

[19] Abdah MAAM, Awan HTA, Mehar M, Mustafa MN, Walvekar R, Alam MW, et al. Advancements in MXene-polymer composites for high-performance supercapacitor applications. J Energy Storage 2023;63:106942.
[20] Riazi H, Nemani SK, Grady MC, Anasori B, Soroush M. Ti3C2 MXene–polymer nanocomposites and their applications. J Mater Chem A 2021;9:8051–98.
[21] Khosla A, Sonu Awan HTA, Singh K, Gaurav WR, et al. Emergence of MXene and MXene–polymer hybrid membranes as future- environmental remediation strategies. Adv Sci 2022;9:2203527.
[22] Kshetri T, Tran DT, Le HT, Nguyen DC, Hoa HV, Kim NH, et al. Recent advances in MXene-based nanocomposites for electrochemical energy storage applications. Prog Mater Sci 2021;117:100733.
[23] Tan KH, Samylingam L, Aslfattahi N, Saidur R, Kadirgama K. Optical and conductivity studies of polyvinyl alcohol-MXene (PVA-MXene) nanocomposite thin films for electronic applications. Opt Laser Technol 2021;136:106772.
[24] Pan Y, Fu L, Zhou Q, Wen Z, Lin C-T, Yu J, et al. Flammability, thermal stability and mechanical properties of polyvinyl alcohol nanocomposites reinforced with delaminated Ti3C2Tx (MXene). Polym Compos 2020;41:210–18.
[25] Eslami R, Azizi N, Santhirakumaran P, Mehrvar M, Zarrin H. 3D dual network effect of alkalinized MXene and hBN in PVA for wearable strain/pressure sensor applications. Chem Eng J 2024;480:148063.
[26] Naguib M, Saito T, Lai S, Rager MS, Aytug T, Parans Paranthaman M, et al. Ti3C2Tx (MXene)–polyacrylamide nanocomposite films. RSC Adv 2016;6:72069–73.
[27] Li X, Peng W, Li L, Chen S, Ye L, Peng C. Simple synthesis of copper/MXene/polyacrylamide hydrogel catalyst for 4-nitrophenol reduction. Mater Lett 2022;324:132705.
[28] Wu J, Chen Y, Zhang L, Sheng X. Electrostatic self-assembled MXene@PDDA-Fe3O4 nanocomposite: a novel, efficient, and stable low-temperature phosphating accelerator. J Ind Eng Chem 2024;129:424–34.
[29] Mazhar S, Qarni AA, Ul Haq Y, Ul Haq Z, Murtaza I. Promising PVC/MXene based flexible thin film nanocomposites with excellent dielectric, thermal and mechanical properties. Ceram Int 2020;46:12593–605.
[30] Qin L, Tao Q, El Ghazaly A, Fernandez-Rodriguez J, Persson POÅ, Rosen J, et al. High-performance ultrathin flexible solid-state supercapacitors based on solution processable Mo1.33C MXene and PEDOT:PSS. Adv Funct Mater 2018;28:1703808.
[31] Yang G-Y, Wang S-Z, Sun H-T, Yao X-M, Li C-B, Li Y-J, et al. Ultralight, conductive Ti3C2Tx MXene/PEDOT:PSS hybrid aerogels for electromagnetic interference shielding dominated by the absorption mechanism. ACS Appl Mater Interfaces 2021;13:57521–31.
[32] Li W, Song Z, Zhong J, Qian J, Tan Z, Wu X, et al. Multilayer-structured transparent MXene/PVDF film with excellent dielectric and energy storage performance. J Mater Chem C 2019;7:10371–8.
[33] Hasan MM, Sadeque MSB, Albasar I, Pecenek H, Dokan FK, Onses MS, et al. Scalable fabrication of MXene-PVDF nanocomposite triboelectric fibers via thermal drawing. Small 2023;19:2206107.
[34] Rajavel K, Luo S, Wan Y, Yu X, Hu Y, Zhu P, et al. 2D Ti3C2Tx MXene/polyvinylidene fluoride (PVDF) nanocomposites for attenuation of electromagnetic radiation with excellent heat dissipation. Compos Part A Appl Sci Manuf 2020;129:105693.
[35] Ronchi RM, Marchiori CFN, Araujo CM, Arantes JT, Santos SF. Thermoplastic polyurethane – Ti3C2(Tx) MXene nanocomposite: the influence of functional groups upon the matrix–reinforcement interaction. Appl Surf Sci 2020;528:146526.
[36] Sheng X, Zhao Y, Zhang L, Lu X. Properties of two-dimensional Ti3C2 MXene/thermoplastic polyurethane nanocomposites with effective reinforcement via melt blending. Compos Sci Technol 2019;181:107710.
[37] Zheng Y, Chen W, Sun Y, Huang C, Wang Z, Zhou D. High conductivity and stability of polystyrene/MXene composites with orientation-3D network binary structure. J Colloid Interface Sci 2021;595:151–8.
[38] Zhang Z, Cao H, Quan Y, Ma R, Pentzer EB, Green MJ, et al. Thermal Stability and Flammability Studies of MXene–Organic Hybrid Polystyrene Nanocomposites. Polymers (Basel) 2022.
[39] Luo J-Q, Zhao S, Zhang H-B, Deng Z, Li L, Yu Z-Z. Flexible, stretchable and electrically conductive MXene/natural rubber nanocomposite films for efficient electromagnetic interference shielding. Compos Sci Technol 2019;182:107754.
[40] Gan Q, Song L, Wang Y, Yuan Q, Huang W, Zhu Y, et al. Towards flexible and healable strain sensors via a modulated interface between Ti3C2 MXene and epoxidized natural rubber. Nano Energy 2024;120:109141.
[41] Shi Y, Liu C, Liu L, Fu L, Yu B, Lv Y, et al. Strengthening, toughing and thermally stable ultra-thin MXene nanosheets/polypropylene nanocomposites via nanoconfinement. Chem Eng J 2019;378:122267.
[42] Purbayanto MAK, Jakubczak M, Bury D, Nair VG, Birowska M, Moszczyńska D, et al. Tunable Antibacterial Activity of a Polypropylene Fabric Coated with Bristling Ti3C2Tx MXene Flakes Coupling the Nanoblade Effect with ROS Generation. ACS Appl Nano Mater 2022;5:5373–86.
[43] Zhang W, Ji X-X, Ma M-G. Emerging MXene/cellulose composites: design strategies and diverse applications. Chem Eng J 2023;458:141402.
[44] Carey M, Barsoum MW. MXene polymer nanocomposites: a review. Mater Today Adv 2021;9:100120.
[45] Han X, Qiu X, Zong M, Hao J. Assembled MXene Macrostructures for Multifunctional Polymer Nanocomposites. Small Struct 2023;4:2300090.
[46] Chen X, Zhao Y, Li L, Wang Y, Wang J, Xiong J, et al. MXene/Polymer Nanocomposites: preparation, Properties, and Applications. Polym Rev 2021;61:80–115.
[47] He S, Sun X, Zhang H, Yuan C, Wei Y, Li J. Preparation Strategies and Applications of MXene-Polymer Composites: a Review. Macromol Rapid Commun 2021;42:2100324.
[48] Idumah CI, Ezeani OE, Okonkwo UC, Nwuzor IC, Odera SR. Novel Trends in MXene/Conducting Polymeric Hybrid Nanoclusters. J Cluster Sci 2023;34:45–76.
[49] Jaya Prakash N, Kandasubramanian B. Nanocomposites of MXene for industrial applications. J Alloys Compd 2021;862:158547.
[50] Oliveira FM, Azadmanjiri J, Wang X, Yu M, Sofer Z. Structure Design and Processing Strategies of MXene-Based Materials for Electromagnetic Interference Shielding. Small Methods 2023;7:2300112.
[51] Zhang Q, Wang Q, Cui J, Zhao S, Zhang G, Gao A, et al. Structural design and preparation of Ti3C2Tx MXene/polymer composites for absorption-dominated electromagnetic interference shielding. Nanoscale Adv 2023;5:3549–74.
[52] Tan X, Yuan Q, Qiu M, Yu J, Jiang N, Lin C-T, et al. Rational design of graphene/polymer composites with excellent electromagnetic interference shielding effectiveness and high thermal conductivity: a mini review. J Mater Sci Technol 2022;117:238–50.
[53] Idowu A, Boesl B, Agarwal A. 3D graphene foam-reinforced polymer composites – a review. Carbon N Y 2018;135:52–71.
[54] Salzano de Luna M, Wang Y, Zhai T, Verdolotti L, Buonocore GG, Lavorgna M, et al. Nanocomposite polymeric materials with 3D graphene-based architectures: from design strategies to tailored properties and potential applications. Prog Polym Sci 2019;89:213–49.
[55] Pang H, Xu L, Yan D-X, Li Z-M. Conductive polymer composites with segregated structures. Prog Polym Sci 2014;39:1908–33.
[56] Zheng S, Wang Y, Zhu Y, Zheng C. Recent advances in the construction and properties of carbon-based nanofillers/polymer composites with segregated network structures. Mater Today Commun 2023;36:106773.
[57] Li G, Wyatt BC, Song F, Yu C, Wu Z, Xie X, et al. 2D Titanium Carbide (MXene) based films: expanding the frontier of functional film materials. Adv Funct Mater 2021;31:2105043.
[58] Wang M, Liu Y, Zhang H, Wu Y, Pan L. Thermal conductivities of Ti3C2Tx MXenes and their interfacial thermal performance in MXene/epoxy composites – a molecular dynamics simulation. Int J Heat Mass Transfer 2022;194:123027.
[59] Kang R, Zhang Z, Guo L, Cui J, Chen Y, Hou X, et al. Enhanced Thermal Conductivity of Epoxy Composites Filled with 2D Transition Metal Carbides (MXenes) with Ultralow Loading. Sci Rep 2019;9:9135.
[60] Liu R, Miao M, Li Y, Zhang J, Cao S, Feng X. Ultrathin Biomimetic Polymeric Ti3C2Tx MXene composite films for electromagnetic interference shielding. ACS Appl Mater Interfaces 2018;10:44787–95.
[61] Wan Y-J, Li X-M, Zhu P-L, Sun R, Wong C-P, Liao W-H. Lightweight, flexible MXene/polymer film with simultaneously excellent mechanical property and high-performance electromagnetic interference shielding. Compos Part A Appl Sci Manuf 2020;130:105764.
[62] Cao W-T, Chen F-F, Zhu Y-J, Zhang Y-G, Jiang Y-Y, Ma M-G, et al. Binary strengthening and toughening of MXene/cellulose nanofiber composite paper with nacre-inspired structure and superior electromagnetic interference shielding properties. ACS Nano 2018;12:4583–93.
[63] Shahzad F, Alhabeb M, Hatter CB, Anasori B, Man Hong S, Koo CM, et al. Electromagnetic interference shielding with 2D transition metal carbides (MXenes). Science 2016;353:1137–40.
[64] Ling Z, Ren CE, Zhao M-Q, Yang J, Giammarco JM, Qiu J, et al. Flexible and conductive MXene films and nanocomposites with high capacitance. Proc Natl Acad Sci 2014;111:16676–81.
[65] Zhang Z, Yang S, Zhang P, Zhang J, Chen G, Feng X. Mechanically strong MXene/Kevlar nanofiber composite membranes as high-performance nanofluidic osmotic power generators. Nat Commun 2019;10:2920.
[66] Ma Z, Kang S, Ma J, Shao L, Zhang Y, Liu C, et al. Ultraflexible and mechanically strong double-layered aramid nanofiber–Ti3C2Tx MXene/silver nanowire nanocomposite papers for high-performance electromagnetic interference shielding. ACS Nano 2020;14:8368–82.
[67] Boota M, Anasori B, Voigt C, Zhao M-Q, Barsoum MW, Gogotsi Y. Pseudocapacitive electrodes produced by oxidant-free polymerization of pyrrole between the layers of 2D Titanium Carbide (MXene). Adv Mater 2016;28:1517–22.
[68] He Z, Xie H, Wu H, Chen J, Ma S, Duan X, et al. Recent advances in MXene/polyaniline-based composites for electrochemical devices and electromagnetic interference shielding applications. ACS Omega 2021;6:22468–77.
[69] VahidMohammadi A, Moncada J, Chen H, Kayali E, Orangi J, Carrero CA, et al. Thick and freestanding MXene/PANI pseudocapacitive electrodes with ultrahigh specific capacitance. J Mater Chem A 2018;6:22123–33.
[70] Wang J, Jiang D, Zhang M, Sun Y, Jiang M, Du Y, et al. Ice crystal-assisted intercalation of PANI within Ti3C2Tx MXene thin films for flexible supercapacitor electrodes with simultaneously high mechanical strength and rate performance. J Mater Chem A 2023;11:1419–29.
[71] Zhou B, Zhang Z, Li Y, Han G, Feng Y, Wang B, et al. Flexible, robust, and multifunctional electromagnetic interference shielding film with alternating cellulose nanofiber and MXene layers. ACS Appl Mater Interfaces 2020;12:4895–905.
[72] Zhou B, Li Q, Xu P, Feng Y, Ma J, Liu C, et al. An asymmetric sandwich structural cellulose-based film with self-supported MXene and AgNW layers for flexible electromagnetic interference shielding and thermal management. Nanoscale 2021;13:2378–88.
[73] Bian X, Yang Z, Zhang T, Yu J, Xu G, Chen A, et al. Multifunctional Flexible AgNW/MXene/PDMS composite films for efficient electromag-

netic interference shielding and strain sensing. ACS Appl Mater Interfaces 2023;15:41906–15.
[74] Lipton J, Weng G-M, Röhr JA, Wang H, Taylor AD. Layer-by-layer assembly of two-dimensional materials: meticulous control on the Nanoscale. Matter. 2020;2:1148–65.
[75] Decher G, Lehr B, Lowack K, Lvov Y, Schmitt J. New nanocomposite films for biosensors: layer-by-layer adsorbed films of polyelectrolytes, proteins or DNA. Biosens Bioelectron 1994;9:677–84.
[76] Borges J, Mano JF. Molecular interactions driving the layer-by-layer assembly of multilayers. Chem Rev 2014;114:8883–942.
[77] Lipton J, Weng G-M, Alhabeb M, Maleski K, Antonio F, Kong J, et al. Mechanically strong and electrically conductive multilayer MXene nanocomposites. Nanoscale 2019;11:20295–300.
[78] Decher G, Hong J-D. Buildup of ultrathin multilayer films by a self-assembly process, 1 consecutive adsorption of anionic and cationic bipolar amphiphiles on charged surfaces. Makromol Chem Macromol Symp 1991;46:321–7.
[79] An H, Habib T, Shah S, Gao H, Radovic M, Green MJ, et al. Surface-agnostic highly stretchable and bendable conductive MXene multilayers. Sci Adv 2018;4:eaaq0118.
[80] Echols IJ, An H, Yun J, Sarang KT, Oh J-H, Habib T, et al. Electronic and optical property control of polycation/MXene layer-by-layer assemblies with chemically diverse MXenes. Langmuir 2021;37:11338–50.
[81] Tian W, VahidMohammadi A, Wang Z, Ouyang L, Beidaghi M, Hamedi MM. Layer-by-layer self-assembly of pillared two-dimensional multilayers. Nat Commun 2019;10:2558.
[82] An H, Habib T, Shah S, Gao H, Patel A, Echols I, et al. Water sorption in MXene/polyelectrolyte multilayers for ultrafast humidity sensing. ACS Appl Nano Mater 2019;2:948–55.
[83] Weng G-M, Li J, Alhabeb M, Karpovich C, Wang H, Lipton J, et al. Layer-by-layer assembly of cross-functional semi-transparent MXene-carbon nanotubes composite films for next-generation electromagnetic interference shielding. Adv Funct Mater 2018;28:1803360.
[84] Echols IJ, An H, Zhao X, Prehn EM, Tan Z, Radovic M, et al. pH-Response of polycation/Ti3C2Tx MXene layer-by-layer assemblies for use as resistive sensors. Mol Syst Des Eng. 2020;5:366–75.
[85] Kharlampieva E, Kozlovskaya V, Sukhishvili SA. Layer-by-layer hydrogen-bonded polymer films: from fundamentals to applications. Adv Mater 2009;21:3053–65.
[86] Fu Y, Bai S, Cui S, Qiu D, Wang Z, Zhang X. Hydrogen-bonding-directed layer-by-layer multilayer assembly: reconformation yielding microporous films. Macromolecules 2002;35:9451–8.
[87] Stockton WB, Rubner MF. Molecular-level processing of conjugated polymers. 4. Layer-by-layer manipulation of polyaniline via hydrogen-bonding interactions. Macromolecules 1997;30:2717–25.
[88] Cheng Y, Xie Y, Cao H, Li L, Liu Z, Yan S, et al. High-strength MXene sheets through interlayer hydrogen bonding for self-healing flexible pressure sensor. Chem Eng J 2023;453:139823.
[89] Meng X, Sun Y, Yu M, Wang Z, Qiu J. Hydrogen-bonding crosslinking MXene to highly robust and ultralight aerogels for strengthening lithium metal anode. Small Sci 2021;1:2100021.
[90] Cheung JH, Stockton WB, Rubner MF. Molecular-level processing of conjugated polymers. 3. Layer-by-layer manipulation of polyaniline via electrostatic interactions. Macromolecules 1997;30:2712–16.
[91] Gong K, Zhou K, Qian X, Shi C, Yu B. MXene as emerging nanofillers for high-performance polymer composites: a review. Compos B Eng 2021;217:108867.
[92] Alfred A, Jamari SS, Mariatti M, Ghazali S. Segregated nanofiller: recent development in polymer-based composites and its applications. In: Mater Today Proc; 2023.
[93] Sun R, Zhang H-B, Liu J, Xie X, Yang R, Li Y, et al. Highly conductive transition metal carbide/carbonitride(MXene)@polystyrene nanocomposites fabricated by electrostatic assembly for highly efficient electromagnetic interference shielding. Adv Funct Mater 2017;27:1702807.
[94] Lv K, Zhang J, Zhao X, Kong N, Tao J, Zhou J. Understanding the effect of pore size on electrochemical capacitive performance of MXene foams. Small 2022;18:2202203.
[95] Lee J, Hong S, Sun Y, Lee SK, Hwang U, Nam J-D, et al. Parasitic reaction driven facile preparation of segregated-MXene/polycarbonate nanocomposites for efficient electromagnetic interference shielding. Surf Interfaces 2023;40:103101.
[96] Zhang Q, Cui J, Zhao S, Zhang G, Gao A, Yan Y. Development of electromagnetic-wave-shielding polyvinylidene fluoride–Ti3C2Tx MXene–carbon nanotube composites by improving impedance matching and conductivity. Nanomaterials 2023.
[97] Wang Y, Liu R, Zhang J, Miao M, Feng X. Vulcanization of Ti3C2Tx MXene/natural rubber composite films for enhanced electromagnetic interference shielding. Appl Surf Sci 2021;546:149143.
[98] Iqbal A, Sambyal P, Kwon J, Han M, Hong J, Kim SJ, et al. Enhanced absorption of electromagnetic waves in Ti3C2Tx MXene films with segregated polymer inclusions. Compos Sci Technol 2021;213:108878.
[99] Zhao M-Q, Xie X, Ren CE, Makaryan T, Anasori B, Wang G, et al. Hollow MXene Spheres and 3D Macroporous MXene Frameworks for Na-Ion Storage. Adv Mater 2017;29:1702410.
[100] Guo Q, Zhang X, Zhao F, Song Q, Su G, Tan Y, et al. Protein-Inspired Self-Healable Ti3C2 MXenes/Rubber-Based Supramolecular Elastomer for Intelligent Sensing. ACS Nano 2020;14:2788–97.
[101] Ma W, Cai W, Chen W, Liu P, Wang J, Liu Z. Microwave-induced segregated composite network with MXene as interfacial solder for ultra-efficient electromagnetic interference shielding and anti-dripping. Chem Eng J 2021;425:131699.
[102] Feng D, Wang Q, Xu D, Liu P. Microwave assisted sinter molding of polyetherimide/carbon nanotubes composites with segregated structure for high-performance EMI shielding applications. Compos Sci Technol 2019;182:107753.
[103] Bian R, Lin R, Wang G, Lu G, Zhi W, Xiang S, et al. 3D assembly of Ti3C2-MXene directed by water/oil interfaces. Nanoscale 2018;10:3621–5.
[104] Shi S, Qian B, Wu X, Sun H, Wang H, Zhang H-B, et al. Self-Assembly of MXene-surfactants at liquid–liquid interfaces: from structured liquids to 3D aerogels. Angew Chem Int editor 2019;58:18171–6.
[105] Cao H, Escamilla M, Anas M, Tan Z, Gulati S, Yun J, et al. Synthesis and electronic applications of particle-templated Ti3C2Tz MXene–polymer films via pickering emulsion polymerization. ACS Appl Mater Interfaces 2021;13:51556–66.
[106] Wang D, Lin Y, Hu D, Jiang P, Huang X. Multifunctional 3D-MXene/PDMS nanocomposites for electrical, thermal and triboelectric applications. Compos Part A Appl Sci Manuf 2020;130:105754.
[107] Yang P, Xia T, Ghosh S, Wang J, Rawson SD, Withers PJ, et al. Realization of 3D epoxy resin/Ti3C2Tx MXene aerogel composites for low-voltage electrothermal heating. 2D Mater 2021;8:025022.
[108] Wang L, Qiu H, Song P, Zhang Y, Lu Y, Liang C, et al. 3D Ti3C2Tx MXene/C hybrid foam/epoxy nanocomposites with superior electromagnetic interference shielding performances and robust mechanical properties. Compos Part A Appl Sci Manuf 2019;123:293–300.
[109] Meng F, Zhang Z, Gao P, Kang R, Boyjoo Y, Yu J, et al. Excellent tribological properties of epoxy—Ti3C2 with three-dimensional nanosheets composites. Friction 2021;9:734–46.
[110] Guo L, Zhang Z, Li M, Kang R, Chen Y, Song G, et al. Extremely high thermal conductivity of carbon fiber/epoxy with synergistic effect of MXenes by freeze-drying. Compos Commun 2020;19:134–41.
[111] Wang L, Song P, Lin C-T, Kong J, Gu J. 3D Shapeable, Superior Electrically Conductive Cellulose Nanofibers/Ti3C2Tx MXene Aerogels/Epoxy Nanocomposites for Promising EMI Shielding. Research. 2020.
[112] Zhang Y, He Y, Zhou Y, Liu M, Wang Y, Yuan J, et al. Fabrication of RGO/CNTs/MXene 3D skeleton structure for enhancing thermal and tribological properties of epoxy composites. Tribol Int 2023;179:108172.
[113] Zhou Y, Zhang Y, Wang J, He Y, Yuan J, Men X. Well-aligned MXene@MoS2/Carbon nanofiber aerogels reinforced epoxy composites with splendid thermal and tribological performance. Carbon N Y 2023;213:118222.
[114] Jin L, Cao W, Wang P, Song N, Ding P. Interconnected MXene/Graphene network constructed by soft template for multi-performance improvement of polymer composites. Nanomicro Lett 2022;14:133.
[115] Shao Y-W, Hu W-W, Gao M-H, Xiao Y-Y, Huang T, Zhang N, et al. Flexible MXene-coated melamine foam based phase change material composites for integrated solar-thermal energy conversion/storage, shape memory and thermal therapy functions. Compos Part A Appl Sci Manuf 2021;143:106291.
[116] Chen J, Mo Z, Chen Y, Mo P, Hu Z, Chen X, et al. Highly Stable MXene-based phase change composites with enhanced thermal conductivity and photothermal storage capability. ACS Appl Energy Mater 2022;5:11669–83.
[117] Li K, Liang M, Wang H, Wang X, Huang Y, Coelho J, et al. 3D MXene architectures for efficient energy storage and conversion. Adv Funct Mater 2020;30:2000842.
[118] Bu F, Zagho MM, Ibrahim Y, Ma B, Elzatahry A, Zhao D. Porous MXenes: synthesis, structures, and applications. Nano Today 2020;30:100803.
[119] Han M, Yin X, Hantanasirisakul K, Li X, Iqbal A, Hatter CB, et al. Anisotropic MXene aerogels with a mechanically tunable ratio of electromagnetic wave reflection to absorption. Adv Opt Mater 2019;7:1900267.
[120] Xu H, Yin X, Li X, Li M, Liang S, Zhang L, et al. Lightweight Ti2CTx MXene/Poly(vinyl alcohol) composite foams for electromagnetic wave shielding with absorption-dominated feature. ACS Appl Mater Interfaces 2019;11:10198–207.
[121] Xie P, Zhang C, Li M, You Q, Yuan Y, Qiu S, et al. Study on Pickering emulsions co-stabilized by multiple particles for building MXene-based multifunctional composite foam. Colloids Surf Physicochem Eng Aspects 2023;676:132090.
[122] Liu J, Zhang H-B, Xie X, Yang R, Liu Z, Liu Y, et al. Multifunctional, Superelastic, and Lightweight MXene/Polyimide Aerogels. Small 2018;14:1802479.
[123] Hu Y, Zhuo H, Luo Q, Wu Y, Wen R, Chen Z, et al. Biomass polymer-assisted fabrication of aerogels from MXenes with ultrahigh compression elasticity and pressure sensitivity. J Mater Chem A 2019;7:10273–81.
[124] Han C, Zhang H, Chen Q, Li T, Kong L, Zhao H, et al. A directional piezoelectric sensor based on anisotropic PVDF/MXene hybrid foam enabled by unidirectional freezing. Chem Eng J 2022;450:138280.
[125] Zhang H, Zhang G, Tang M, Zhou L, Li J, Fan X, et al. Synergistic effect of carbon nanotube and graphene nanoplates on the mechanical, electrical and electromagnetic interference shielding properties of polymer composites and polymer composite foams. Chem Eng J 2018;353:381–93.
[126] Liu J, Zhang H-B, Sun R, Liu Y, Liu Z, Zhou A, et al. Hydrophobic, Flexible, and Lightweight MXene foams for high-performance electromagnetic-interference shielding. Adv Mater 2017;29:1702367.
[127] Su T, Liu N, Gao Y, Lei D, Wang L, Ren Z, et al. MXene/cellulose nanofiber–foam based high performance degradable piezoresistive sensor with greatly expanded interlayer distances. Nano Energy 2021;87:106151.
[128] Zhao B, Wu H, Tian Q, Li Y, Qiu F, Zhang T. Laminated MXene Foam/Cellulose@LDH composite membrane with efficient EMI shielding prop-

erty for asymmetric personal thermal management. ACS Appl Mater Interfaces 2023;15:8751–60.
[129] Yin T, Cheng Y, Hou Y, Sun L, Ma Y, Su J, et al. 3D porous structure in MXene/PANI foam for a high-performance flexible pressure sensor. Small 2022;18:2204806.
[130] Cheng H, Pan Y, Li W, Liu C, Shen C, Liu X, et al. Facile design of multifunctional melamine foam with Ni-anchored reduced graphene oxide/MXene as highly efficient microwave absorber. Nano Today 2023;52:101958.
[131] Li R, Ding L, Gao Q, Zhang H, Zeng D, Zhao B, et al. Tuning of anisotropic electrical conductivity and enhancement of EMI shielding of polymer composite foam via CO2-assisted delamination and orientation of MXene. Chem Eng J 2021;415:128930.
[132] Dehghan P, Simiari M, Gholampour M, Aghvami-Panah M, Amirkiai A. Tuning the electromagnetic interference shielding performance of polypropylene cellular nanocomposites: role of hybrid nanofillers of MXene and reduced graphene oxide. Polym Test 2023;126:108162.
[133] Yue Y, Liu N, Liu W, Li M, Ma Y, Luo C, et al. 3D hybrid porous Mxene-sponge network and its application in piezoresistive sensor. Nano Energy 2018;50:79–87.
[134] Ma W, Cai W, Chen W, Liu P, Wang J, Liu Z. A novel structural design of shielding capsule to prepare high-performance and self-healing MXene-based sponge for ultra-efficient electromagnetic interference shielding. Chem Eng J 2021;426:130729.
[135] Li L, Liu X, Wang J, Yang Y, Cao Y, Wang W. New application of MXene in polymer composites toward remarkable anti-dripping performance for flame retardancy. Compos Part A Appl Sci Manuf 2019;127:105649.
[136] Zhang M, Yang W, Wang Z, Liu H, Yin R, Liu C, et al. Highly compressible and thermal insulative conductive MXene/PEDOT:PSS@melamine foam for promising wearable piezoresistive sensor. Appl Phys Lett 2023;122:043507.
[137] Kim E, Zhang H, Lee J-H, Chen H, Zhang H, Javed MH, et al. MXene/polyurethane auxetic composite foam for electromagnetic interference shielding and impact attenuation. Compos Part A Appl Sci Manuf 2021;147:106430.
[138] Jia X, Shen B, Zhang L, Zheng W. Construction of compressible Polymer/MXene composite foams for high-performance absorption-dominated electromagnetic shielding with ultra-low reflectivity. Carbon N Y 2021;173:932–40.
[139] Xu Z, Ding X, Li S, Huang F, Wang B, Wang S, et al. Oxidation-Resistant MXene-based melamine foam with ultralow-percolation thresholds for electromagnetic-infrared compatible shielding. ACS Appl Mater Interfaces 2022;14:40396–407.
[140] Li Z, Sun Y, Zhou B, Feng Y, Liu C, Shen C. Flexible thermoplastic polyurethane/MXene foams for compressible electromagnetic interference shielding. Mater Today Phys 2023;32:101017.
[141] Lin B, Yuen ACY, Li A, Zhang Y, Chen TBY, Yu B, et al. MXene/chitosan nanocoating for flexible polyurethane foam towards remarkable fire hazards reductions. J Hazard Mater 2020;381:120952.
[142] Tian Y, Yang C, Que W, He Y, Liu X, Luo Y, et al. Ni foam supported quasi–core-shell structure of ultrathin Ti3C2 nanosheets through electrostatic layer-by-layer self-assembly as high rate-performance electrodes of supercapacitors. J Power Sources 2017;369:78–86.
[143] Hu Y, Chen Z, Ding Y, Xu Y, Lin H, Yu W, et al. Nanofiltration membranes fabricated by plant polyphenol-intermediated MXene and polyethyleneimine layer-by-layer self-assembly for efficient dye/salt separation. Sep Purif Technol 2023;323:124343.
[144] Lin B, Yuen ACY, Oliver S, Liu J, Yu B, Yang W, et al. Dual functionalisation of polyurethane foam for unprecedented flame retardancy and antibacterial properties using layer-by-layer assembly of MXene chitosan with antibacterial metal particles. Compos B Eng 2022;244:110147.
[145] Yun J, Echols I, Flouda P, Wang S, Easley A, Zhao X, et al. Layer-by-layer assembly of polyaniline nanofibers and MXene thin-film electrodes for electrochemical energy storage. ACS Appl Mater Interfaces 2019;11:47929–38.
[146] Wu X, Han B, Zhang H-B, Xie X, Tu T, Zhang Y, et al. Compressible, durable and conductive polydimethylsiloxane-coated MXene foams for high-performance electromagnetic interference shielding. Chem Eng J 2020;381:122622.
[147] Yi W, Wu H, Wang H, Du Q. Interconnectivity of macroporous hydrogels prepared via graphene oxide-stabilized pickering high internal phase emulsions. Langmuir 2016;32:982–90.
[148] Pang B, Liu H, Liu P, Peng X, Zhang K. Water-in-oil Pickering emulsions stabilized by stearoylated microcrystalline cellulose. J Colloid Interface Sci 2018;513:629–37.
[149] Zheng Z, Zhao Y, Ye Z, Hu J, Wang H. Electrically conductive porous MXene-polymer composites with ultralow percolation threshold via Pickering high internal phase emulsion templating strategy. J Colloid Interface Sci 2022;618:290–9.
[150] Fan Q, Yi M, Chai C, Li W, Qi P, Wang J, et al. Oxidation stability enhanced MXene-based porous materials derived from water-in-ionic liquid Pickering emulsions for wearable piezoresistive sensor and oil/water separation applications. J Colloid Interface Sci 2022;618:311–21.
[151] Cao H, Wang Y, Sarmah A, Liu K-W, Tan Z, Arole KD, et al. Electrically conductive porous Ti3C2Tx MXene-polymer composites from high internal phase emulsions (HIPEs). 2D Mater 2022;9:044004.
[152] Cao H, Escamilla M, Arole KD, Holta D, Lutkenhaus JL, Radovic M, et al. Flocculation of MXenes and their use as 2D particle surfactants for capsule formation. Langmuir 2021;37:2649–57.
[153] Wu Z, Shi J, Song P, Li J, Cao S. Chitosan/hyaluronic acid based hollow microcapsules equipped with MXene/gold nanorods for synergistically enhanced near infrared responsive drug delivery. Int J Biol Macromol 2021;183:870–9.
[154] Wang Y, Cipriani C, Hsieh C-M, Cao H, Sarmah A, Liu K-W, et al. Morphology map-guided identification of bijel ink for producing conductive porous structures. Matter 2023;6:4066–85.
[155] Luo Q, Wang Y, Chen Z, Wei P, Yoo E, Pentzer E. Pickering emulsion-templated encapsulation of ionic liquids for contaminant removal. ACS Appl Mater Interfaces 2019;11:9612–20.
[156] Ma X, Wang P, Tian X, Wei Z, Pan J. Ionic liquids filled hybrid capsules by harnessing interfacial imine chemistry of Janus nanosheets stabilized pickering emulsion for removal of chlorophenols. Sep Purif Technol 2022;280:119834.
[157] Lak SN, Ahmed S, Shamberger PJ, Pentzer EB. Encapsulation of hygroscopic liquids via polymer precipitation in non-aqueous emulsions. J Colloid Interface Sci 2022;628:605–13.
[158] Huang Q, Luo Q, Wang Y, Pentzer E, Gurkan B. Hybrid ionic liquid capsules for rapid CO2 capture. Ind Eng Chem Res 2019;58:10503–9.
[159] Lee Y-Y, Edgehouse K, Klemm A, Mao H, Pentzer E, Gurkan B. Capsules of reactive ionic liquids for selective capture of carbon dioxide at low concentrations. ACS Appl Mater Interfaces 2020;12:19184–93.
[160] Gaur SS, Edgehouse KJ, Klemm A, Wei P, Gurkan B, Pentzer EB. Capsules with polyurea shells and ionic liquid cores for CO2 capture. J Polym Sci 2021;59:2980–9.
[161] Shuck CE, Han M, Maleski K, Hantanasirisakul K, Kim SJ, Choi J, et al. Effect of Ti3AlC2 MAX phase on structure and properties of resultant Ti3C2Tx MXene. ACS Appl Nano Mater 2019;2:3368–76.
[162] Athavale S, Micci-Barreca S, Arole K, Kotasthane V, Blivin J, Cao H, et al. Advances in the chemical stabilization of MXenes. Langmuir 2023;39:918–28.